Redox Biology 81 (2025) 103567

Contents lists available at ScienceDirect

Redox Biology

journal homepage: www.elsevier.com/locate/redox

Suppression of the LKB1-AMPK-SLC7A11-GSH signaling pathway sensitizes NSCLC to albumin-bound paclitaxel via oxidative stress

Dade Rong [a], Liangliang Gao [a], Yiguan Chen [a], Xiang-Zheng Gao [a], Mingzhu Tang [a], Haimei Tang [a,b], Yuan Gao [a], Guang Lu [c], Zhi-Qiang Ling [d], Han-Ming Shen [a,*]

[a] Faculty of Health Sciences, Ministry of Education Frontiers Science Center for Precision Oncology, University of Macau, Macau, China
[b] Department of Immunology, Shenzhen University School of Medicine, Shenzhen, China
[c] Department of Physiology, Zhongshan School of Medicine, Sun Yat-sen University, Guangzhou, China
[d] Experimental Research Centre, The Cancer Hospital of the University of Chinese Academy of Sciences, Zhejiang Cancer Hospital, Institute of Basic Medicine and Cancer (IBMC), Chinese Academy of Sciences, Hangzhou, Zhejiang, 310022, China

ARTICLE INFO

Keywords:
Albumin-bound paclitaxel
LKB1
Non-small lung cancer
AMPK
SLC7A11
ROS

ABSTRACT

Albumin-bound paclitaxel (nab-PTX) is an important chemotherapeutic drug used for the treatment of advanced and metastatic non-small cell lung cancer (NSCLC). One critical issue in its clinical application is the development of resistance; thus, a deeper understanding of the mechanisms underlying the primary resistance to nab-PTX is expected to help to develop effective therapeutic strategies to overcome resistance. In this study, we made an unexpected discovery that NSCLC with wild-type (WT) Liver kinase B1 (LKB1), an important tumor suppressor and upstream kinase of AMP-activated protein kinase (AMPK), is more resistant to nab-PTX than NSCLC with mutant *LKB1*. Mechanistically, LKB1 status does not alter the intracellular concentration of nab-PTX or affect its canonical pharmacological action in promoting microtubule polymerization. Instead, we found that LKB1 mediates AMPK activation, leading to increased expression of SLC7A11, a key amino acid transporter and intracellular level of glutathione (GSH), which then attenuates the production of reactive oxygen species (ROS) and apoptotic cell death induced by nab-PTX. On the other hand, genetic or pharmacological inhibition of AMPK in *LKB1*-WT NSCLC reduces the expression of SLC7A11 and intracellular GSH, increases ROS level, and eventually promotes the apoptotic cell death induced by nab-PTX *in vitro*. Consistently, the combination of nab-PTX with an AMPK inhibitor exhibits a greater therapeutic efficacy in *LKB1*-WT NSCLC using xenograft models *in vivo*. Taken together, our data reveal a novel role of LKB1-AMPK-SLC7A11-GSH signaling pathway in the primary resistance to nab-PTX, and provide a therapeutic strategy for the treatment of *LKB1*-WT NSCLC by targeting the LKB1-AMPK-SLC7A11-GSH pathway.

1. Introduction

Lung cancer, as a highly heterogeneous disease, is one of the most common carcinomas and the leading cause of cancer-related death in the world [1]. Histologically, lung cancer can be divided into small cell lung cancer (SCLC) and non-small cell lung cancer (NSCLC) [2] with the latter accounting for approximately 85 % of all lung cancers [2]. Previously, the management of lung cancer was anchored to chemotherapy, radiotherapy and surgery operation [2,3]. With the advancement of lung cancer research, an increasing number of genetic alterations have been discovered, including tumor driver genes (*EGFP*, *KRAS*, *ROS1*) and immune checkpoint proteins (*PD-L1*), which significantly promote the development of targeted therapy and immunotherapy in NSCLC [2,4]. Despite the significant advantages of targeted therapy and immunotherapy in improving the overall prognosis of the patients with NSCLC, there are several important limitations, such as toxicity, drug resistance, and high cost [5]. Meanwhile, targeted therapy and immunotherapy are typically used in combination with chemotherapy in clinical settings [6,7]. Therefore, chemotherapeutic drugs still play an important role in the treatment of lung cancer, especially metastatic lung cancer [2,8,9]. Among these, albumin-bound paclitaxel (nab-PTX) is a widely used chemotherapeutic drug for the treatment of advanced and metastatic NSCLC [2,8,9].

Paclitaxel (PTX), a microtubule-binding drug, is well known to bind

* Corresponding author.
E-mail address: hmshen@um.edu.mo (H.-M. Shen).

https://doi.org/10.1016/j.redox.2025.103567
Received 24 January 2025; Accepted 24 February 2025
Available online 25 February 2025

to β-tubulin to stabilize the microtubules of cells [10], which blocks the dynamics of microtubules [11] and induces apoptosis in cancer cells [12,13]. Nab-PTX is a novel formulation in which PTX binds to albumin nanoparticle through a non-covalent interaction [14,15]. By using albumin as an alternative vehicle for PTX, the allergic reactions induced by CrEL, a solvent to maintain the solubility and stability of PTX, can be avoided, and the efficacy of PTX could be increased for the accumulation of nab-PTX around the tumor by albumin [16]. Currently, nab-PTX is approved by the U.S. Food and Drug Administration (FDA) for the treatment of metastatic breast cancer, locally advanced or metastatic non-small cell lung cancer, and advanced pancreatic cancer [16]. The therapeutic efficacy of nab-PTX has been widely reported [17,18]. Nevertheless, primary or acquired resistance to nab-PTX is a major issue that limits its clinical application. Multiple mechanisms underlying this resistance have been reported, including the upregulation of Mcl-1 [19], sustained induction of c-MYC [20], and overexpression of ABCB1 [21].

Liver kinase B1 (LKB1), a serine/threonine kinase, is a highly mutated gene in NSCLC, with a mutation rate of approximately 15 % [22]. LKB1 is usually regarded as a tumor suppressor: its loss-of-function mutation is responsible for the inherited tumor disorder Peutz-Jeghers syndrome (PJS), in which polyps form in the colon and the persons with PJS have a high risk for developing digestive cancer [23]. The main physiological function of LKB1 is to directly phosphorylate and activate AMP-activated protein kinase (AMPK) at the Thr-172 residue of AMPK α-catalytic subunit [24]. AMPK is probably one of the most important kinases in the control of metabolism, and activated AMPK is capable of promoting catabolism and inhibiting anabolic processes via direct phosphorylation of an array of key target proteins such as mammalian target of rapamycin complex 1 (mTORC1) and acetyl-CoA carboxylase (ACC) [24]. As a downstream effector of LKB1, AMPK is presumably also a tumor suppressor, and activation of AMPK has been considered a potential therapeutic strategy for cancer [24]. However, intriguingly, some studies have reported that the activation of LKB1-AMPK signaling pathway protects the cells against multiple stimulus including energy starvation, nutrition deprivation, hypoxia and oxidative stress [25–32]. Therefore, the suppression of the LKB1-AMPK pathway may serve as a potential therapeutic strategy for cancer.

In this study, we demonstrate that the LKB1-AMPK-SLC7A11-GSH signaling pathway plays an important role in determining the therapeutic efficacy of nab-PTX: In *LKB1*-WT NSCLC cells, activation of LKB1-AMPK signaling promotes the expression of SLC7A11, increases the intracellular GSH level, reduces intracellular ROS level, and thereby impairs the therapeutic efficacy of nab-PTX. Suppression of AMPK significantly sensitizes *LKB1*-WT NSCLC cells to cell death induced by nab-PTX both *in vitro* and *in vivo*. Thus, our study provides experimental evidence that targeting the LKB1-AMPK-SLC7A11-GSH pathway could be a novel therapeutic regimen to overcome the primary resistance to nab-PTX in *LKB1*-WT NSCLC.

2. Materials and methods

2.1. Cells and cell culture

H1299, A549, H460, H1975, H1650, HCC827, H23, H358 and HEK-293T cells were obtained from American Tissue Culture Collection (USA). Except HEK-293T cells, all cell lines were cultured in RPMI (Gibco, 11875093) supplemented with 10 % FBS (Gibco, 10099141C) and 1 % antibiotics (Penicillin/Streptomycin, Gibco, 15140122). HEK-293T cells were cultured in DMEM (Gibco, 11965092) supplemented with 10 % FBS (Gibco, 10099141C) and 1 % antibiotics (Penicillin/Streptomycin, Gibco, 15140122).

2.2. Cell viability measurement

The cells were seeded at a density of 1000 cells/well in 96-well plates and incubated overnight. Following treatment, cell viability was measured using a Cell Counting Kit-8 (Dojindo, CK04) according to the manufacturer's protocol, and the IC_{50} was calculated using GraphPad Prism 7 software.

2.3. Immunoblotting assay

The cells were washed twice with cold PBS, scraped off in RIPA buffer (containing 1 % PMSF), and incubated on ice for 30 min. The cell lysates were centrifuged at 14,000×*g* for 15 min, and the supernatants were stored at −80 °C until further analysis. Protein concentrations were measured using a bicinchoninic acid (BCA) protein assay (Bio-Rad, 5000201). Proteins were denatured by boiling and separated using 12 % SDS-PAGE. Proteins were transferred to PVDF membranes, which were activated in methanol. Membranes were immunoblotted with primary antibodies, followed by incubation with HRP-conjugated secondary anti-rabbit (AlpVHHs, 025-102-005) and anti-mouse (AlpVHHs, 001-101-001) antibodies. The membranes were incubated with Western Chemiluminescent HRP Substrate (Millipore, WBLUF0500) for 1 min and then detected using a ChemiDoc™ Touch Imaging System (Bio-Rad). All antibodies were used at a 1:1000 dilution in 5 % bovine serum albumin (BSA) in TBST buffer for immunoblotting. The primary antibodies for this study are listed in the Antibody section of supplementary materials.

2.4. Immunofluorescence staining

H1299 (sgC and sgLKB1) cells and A549 (EV, LKB1-WT, LKB1-KD) cells were seeded into 12-well plates with coverslips in each well and cultured overnight. Following treatment, the cells were incubated with 5 % BSA for 1 h to suppress nonspecific binding after washing and fixing with 4 % PFA for 30 min at room temperature. Cells were subsequently incubated with anti-rabbit β-tubulin primary antibody (1:100) (Cell Signaling, 2118S) at 4 °C overnight, followed by incubation with goat anti-rabbit IgG (H + L) conjugated to Alexa Fluor^{FM} Plus 488 secondary antibody (1:300) (Thermo, A32731) for 1 h at room temperature. The stained cells were mounted with mounting medium containing DAPI for 5 min and visualized under a confocal microscope (Zeiss LSM710). The β-tubulin channel (green) and DAPI (blue) were photographed and merged using ZEN Microscopy software.

2.5. Cell death measurement

Cells were seeded in 6-well plates and cultured overnight. Following treatment, cell death was measured using an apoptosis kit (Bestbio, BB-4101-100T), according to the manufacturer's protocol. Briefly, the cells were harvested and washed carefully with cold PBS for 1 time. Annexin V-binding solution (400 μL) and 3 μL FITC dye were added, and the cells were incubated for 15 min on ice, followed by the addition of 5 μL PI dye and 1 min of incubation. The cells were immediately analyzed by flow cytometry (Cytoexpert, Beckman Coulter).

2.6. Cell cycle measurement

Cells were seeded in 6-well plates and cultured overnight. After treatment, the cells were collected, washed carefully with PBS, and fixed with 75 % ethanol at −20 °C. After 24 h of fixation, the cells were washed with PBS and stained with propidium iodide (PI) using the Cell Cycle Analysis Kit (Best Bo, BB-4104) for 20 min. The cell cycle features were analyzed using a Cytoflex flow cytometer (Cytoexpert, Beckman Coulter). Data was analyzed using FlowJo 7.6 software.

2.7. Immunohistochemical assay

All xenograft tumors were fixed with 4 % PFA (Beyotime Biotechnology) overnight at 4 °C and then embedded in paraffin. The samples were subsequently sectioned into thin slices and mounted on slides,

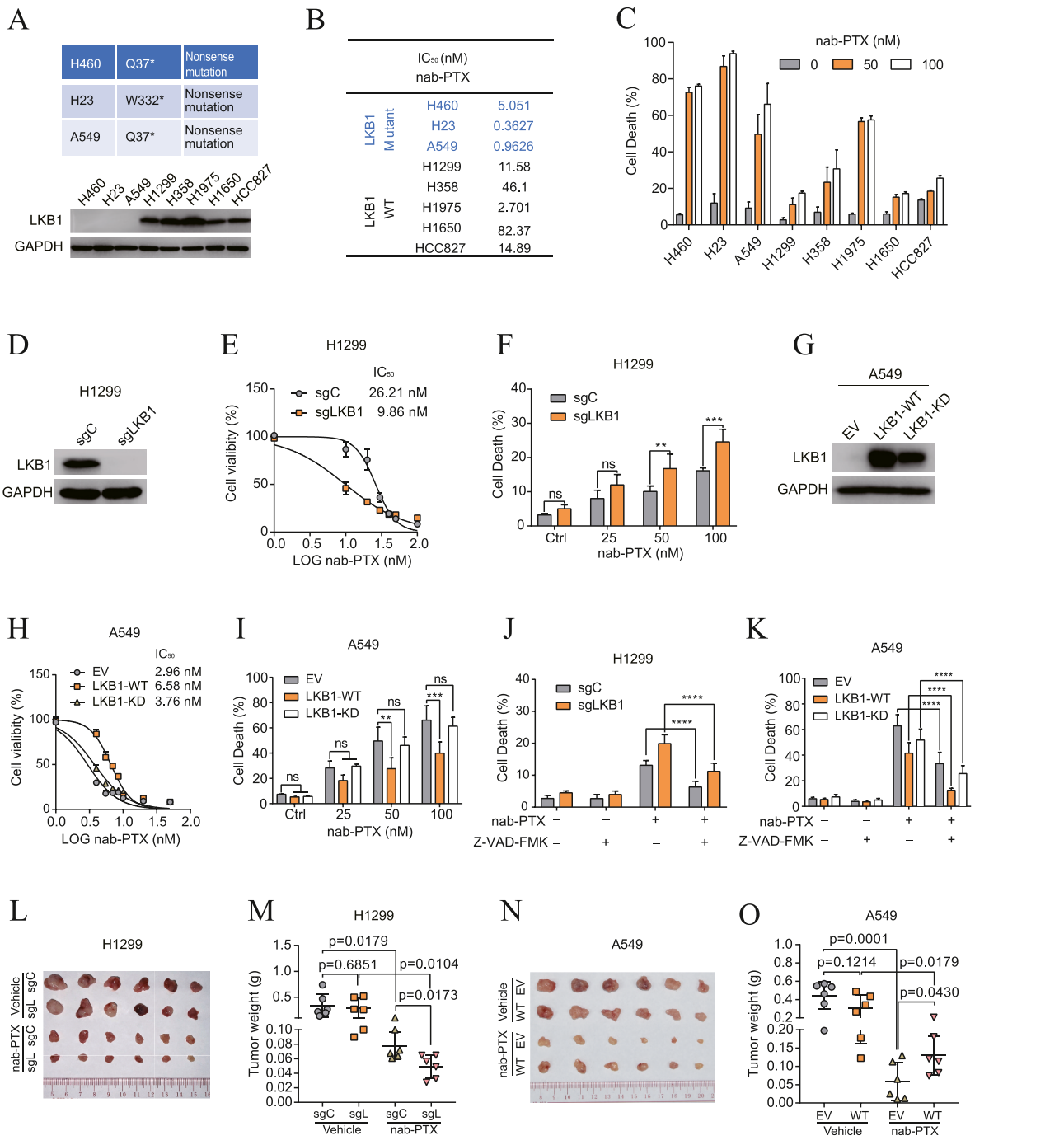

Fig. 1. LKB1 impairs the apoptotic cell death induced by nab-PTX in NSCLC.
A. The genetic alteration of LKB1 in H460, H23 and A549 cells, and an immunoblot showing the level of LKB1 in various NSCLC cell lines. **B.** The IC_{50} values of nab-PTX in various NSCLC cell lines. **C.** Cell death measurement in various NSCLC cell lines treated with indicated concentrations of nab-PTX for 36 h. **D.** An immunoblot showing the deletion of LKB1 in H1299. **E.** Cell viability measurement in indicated H1299 cells treated with indicated concentrations of nab-PTX for 72 h. **F.** Cell death measurement in indicated H1299 cells treated with indicated concentrations of nab-PTX for 36 h. **G.** An immunoblot showing the levels of LKB1 in A549 cells as indicated. **H.** Cell viability measurement in indicated A549 cells treated with indicated concentrations of nab-PTX for 72 h. **I.** Cell death measurement in indicated A549 cells treated with indicated concentrations of nab-PTX for 36 h. **J-K.** Cell death measurement in indicated H1299 cells (**J**) and in indicated A549 cells (**K**) treated with 50 nM nab-PTX combined with or without 20 μM Z-VAD-FMK for 36 h. **L.** Images of the indicated H1299 xenografted tumors at the endpoint of treatment with or without nab-PTX. **M.** Mass of the indicated H1299 xenografted tumors as shown in **L**. **N.** Images of the indicated A549 xenografted tumors at the endpoint of treatment with or without nab-PTX. **O.** Mass of the indicated A549 xenografted tumors as shown in **N**. sgC, sgCtrl; sgL, sgLKB1; EV, empty vector; WT, wide type; KD, kinase dead. ns, no statistical significance; $^{**}p < 0.01$; $^{***}p < 0.001$. The mean ± s.d. are shown; $n \geq 3$ independent experiments. Statistical analysis was performed using an unpaired, two-tailed *t*-test.

followed by deparaffinization in xylene and rehydration using a series of ethanol-water solutions. Antigen retrieval was performed by immersing the sections in citrate–acid buffer and heating them in a microwave oven. The slides were then blocked with 3 % hydrogen peroxide to block nonspecific activity. After rinsing, the slides were blocked with 5 % BSA and then incubated with Ki-67 (Cell Signaling, 9449T), *p*-ACC (Cell Signaling, 11818s), and p-H2A.X (Cell Signaling, 9718S) antibodies overnight at 4 °C. An immunohistochemical staining kit (BOSTER Biological Technology, Wuhan, China) was used for development. Microscopic images (Nikon, Japan) were captured and analyzed by experienced pathologists.

2.8. Gene expression profiling

Gene mutation data for the LUAD cases were obtained using cBioPortal (https://www.cbioportal.org/). Gene expression data for H1650 cells (GSE69747) were obtained from the Gene Expression Omnibus (GEO) database (https://www.ncbi.nlm.nih.gov/geo/). RNA sequencing of A549 and H1299 cells was performed by Novogene. Differentially expressed gene (DEGs) analysis was performed using the limma package. Gene set enrichment analysis (GSEA) was performed using GSEA software (Broad Institute).

2.9. ROS detection

The cells were seeded in a 12-well plate and grown overnight before drug treatment. After treatment, CellROX Oxidative Stress Reagents (Thermo Fisher Scientific, C10444) were added to the cells at a final concentration of 5 μM and incubated for 30 min at 37 °C. After incubation, the cells were harvested through trypsinization. The cells were centrifuged at 300×*g* for 5 min at 4 °C and washed twice with cold PBS. The cells were resuspended in 300 μL cold PBS and subjected to flow cytometry (Cytoexpert, Beckman Coulter) for ROS detection. Data was analyzed using FlowJo_V10 software.

2.10. Glutathione measurements

Cells were seeded at a density of 1×10^4 cells per well in a 96-well plate (Corning, CLS3610) and grown overnight before the measurement of glutathione. Cells were seeded at a density of 5×10^3 cells per well in a 96-well plate (Corning, CLS3610) and grown overnight before treating with vehicle or 20 μM DL-Buthionine-(S,R)-sulfoximine hydrochloride (BSO, MCE, HY-106376B) or 40 μM EX229 (MCE, HY-112769) for 24 h. Glutathione levels were quantified using the GSH-Glo™ Glutathione Assay kit (Promega, V6912) according to manufacturer's instructions. Total levels of glutathione were normalized to protein concentrations as determined by BCA assay.

2.11. RNA extraction and real Time-PCR (RT-PCR)

Cells were seeded in 6-well plates and cultured overnight. According to the instructions of the manufacturer, total RNA was extracted from cultured cells using TRIzol™ Reagent (Invitrogen, 15596026). Total RNA was reverse-transcribed into cDNA using the iScript™ cDNA Synthesis Kits (BIO-RAD, 1708891). RT-PCR was performed with SsoAdvanced Universal SYBR® Green Supermix (BIO-RAD, 1725274) using standard conditions on the 7500 Fast Real-Time PCR system (Life Technologies). GAPDH was served as an internal control for normalization of target mRNA. Relative qPCR primers are shown in Supplementary Materials.

2.12. Plasmid constructions

The CA-AMPK construct was a gift from Prof. Gang Li (addgene, #27632). The CA-AMPK sequence was cloned into the pCDH-CMV plasmid (addgene, #72265) using canonical digestion and ligation assay. pLV3-CMV-SLC7A11(human)-FLAG-Puro (Miaolingbio, P46407) was used for the overexpression of SLC7A11. pLVX-U6-SLC7A11 (human)-shRNA1-PGK-EGFP-Puro (Miaolingbio, P33198) and pLVX-U6-SLC7A11(human)-shRNA2-PGK-EGFP-Puro (Miaolingbio, P33255) were used for the knockdown of SLC7A11.

2.13. CRISPR–Cas9-mediated gene knockout

Knockout of *AMPKα1/α2* in human H1299 cells was performed using single guide RNAs (sgRNAs) and CRISPR–Cas9 technology. pLenti-Puro-sgAMPKα1 (Miaolingbio, P21236) and pLenti-Puro-sgAMPKα2 (Miaolingbio, P21235) were transfected into HEK293T cells with the psPAX2 packaging plasmid (addgene, #12260) and pVSV-G envelope-expressing plasmid (addgene, #138479) by using PEI MAX® (Polysciences, 24765). Supernatant (lentivirus) was collected and stored at −80 °C until ready to use. H1299 cells were infected with lentivirus for 48 h and selected with 2 μg/ml puromycin (Sigma, P9620) for 5 days, and then single cells were sorted into 96-well plates. Single cells were maintained in RPMI with 10 % (v/v) FBS and 1 % (v/v) penicillin/streptomycin at 37 °C in an incubator with 5 % CO2 for 3–4 weeks, and each colony was verified by Immunoblotting.

2.14. Tumor xenograft experiments

Male BALB/c nude mice (4–5 weeks) were purchased from the Animal Facility of the University of Macau. Cancer cells (5×10^5 cells in 180 μL of PBS) were subcutaneously inoculated into the flanks of BALB/c nude mice. Tumor volumes were measured by calipers every other day and calculated using the following formula: $a^2 \times b \times 0.5$, where a represents the smallest diameter and b is the diameter perpendicular to a. Mice were randomly split into two groups receiving either vehicle or nab-PTX (10 mg/kg) combined with or without BAY-3827 (10 mg/kg) every other day for 2 weeks. After the drug treatment period, mice were euthanized by using CO_2 asphyxiation. The xenografts were dissected, weighed, and preserved in a −80 °C freezer for immunohistochemical analysis of cell proliferation and cell death. Animal study was approved by the Ethics Committee of University of Macau (Approved protocol ID: UMARE-009-2022).

2.15. Statistical analysis

All experiments were independently repeated more than two times with similar results. The statistical analyses were performed with GraphPad Prism 7 software. p values are indicated in figures and figure legends. $P < 0.05$ was considered statistically significant.

3. Results

3.1. LKB1 attenuates the therapeutic potency of nab-PTX in NSCLC

A recent study reported that *Kras*-mutant NSCLC cells are more sensitive to the treatment of nab-PTX caused by the enhanced uptake of nab-PTX by activating the MEF/ERK signaling pathway [33]. Co-occurrence of *KRAS* and *LKB1* mutations is a common molecular feature in NSCLC, as summarized in Table S1. Therefore, we deduced that NSCLC with mutant *LKB1* might be more vulnerable to nab-PTX treatment. To verify our hypothesis, we performed the CCK-8 assay to determine the IC_{50} value of nab-PTX in a panel of NSCLC cell lines. The results showed that *LKB1*-mutant NSCLC cells were generally more sensitive to nab-PTX than those NSCLC cells with wide type (WT) *LKB1* (Fig. 1A and B). The results of the cell death assay also showed that nab-PTX displayed more potent cytotoxicity in *LKB1*-mutant NSCLC cells (Fig. 1C). To establish a causal relationship between LKB1 and nab-PTX cytotoxicity, we manipulated LKB1 status in NSCLC cells. First, deletion of *LKB1* in H1299 cells (a cell line with WT-*LKB1*) using CRISPR/Cas9 technology (Fig. 1D) significantly increased the efficacy of

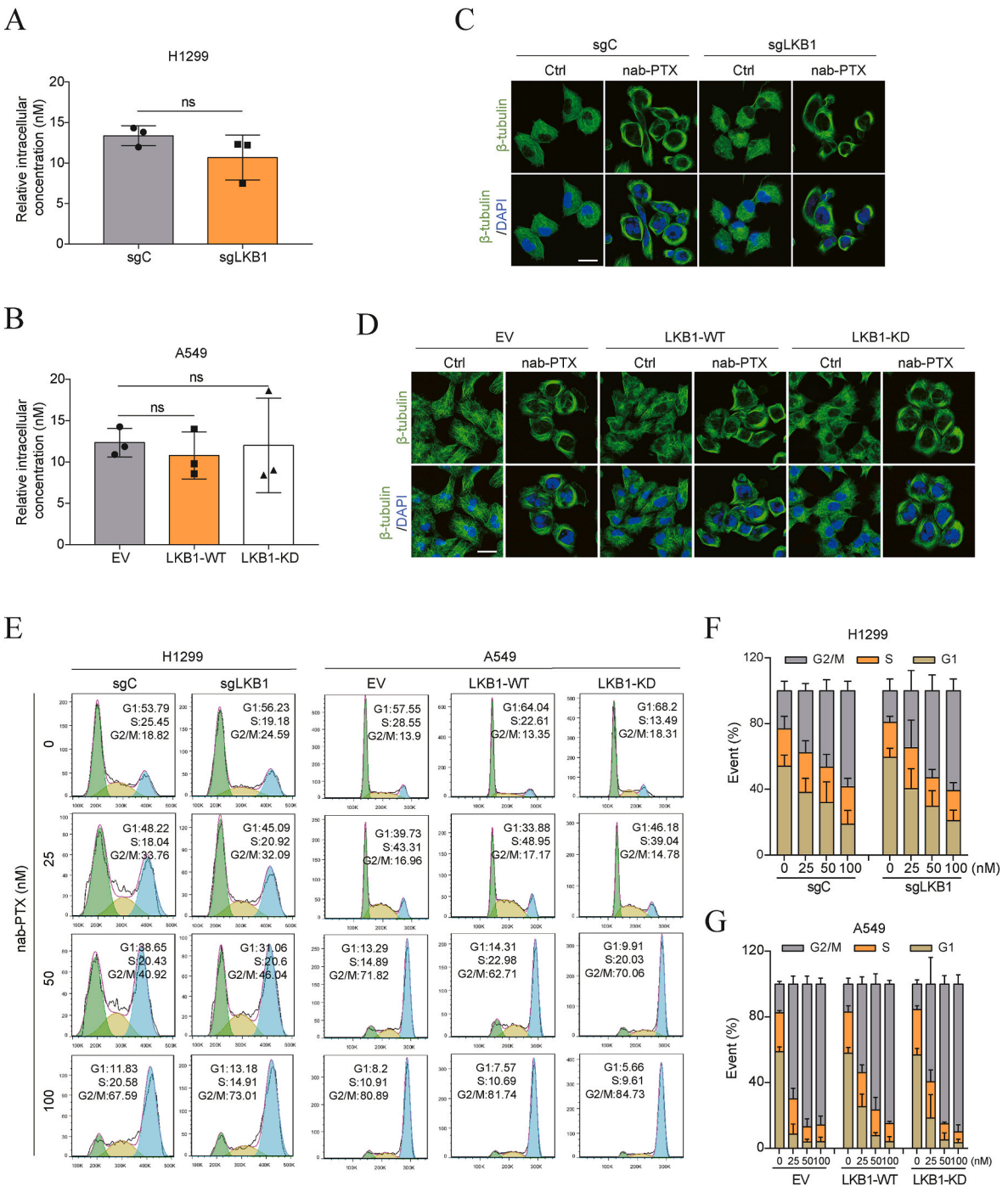

Fig. 2. LKB1 does not affect the uptake of nab-PTX and its canonical pharmacological effects

A-B. Intracellular concentration measurement of PTX in indicated H1299 cells (**A**) and in indicated A549 cells (**B**) upon treatment with 50 nM nab-PTX for 6 h. **C-D.** Confocal microscopy images of microtubule distribution in indicated H1299 cells (**C**) and in indicated A549 cells (**D**) treated with 50 nM nab-PTX for 16 h. Green: β-tubulin; blue: nuclei with DAPI. **E.** Cell cycle measurement in indicated H1299 cells and in indicated A549 cells treated with 50 nM nab-PTX for 16 h. **F-G.** Statistical analyses of cell cycle measurements in indicated H1299 cells (**F**) and in indicated A549 cells (**G**) treated as **E.** sgC, sgCtrl; sgL, sgLKB1; EV, empty vector; WT, wide type; KD, kinase dead. Scale bar, 10 μM. ns, no statistical significance. The mean ± s.d. are shown; n = 3 independent experiments. Statistical analysis was performed using an unpaired, two-tailed *t*-test.

nab-PTX (Fig. 1E and F). Conversely, overexpression of WT-LKB1, but not its kinase-dead (KD) form, in A549 (a cell line with mutant *LKB1*) cells (Fig. 1G) obviously reduced the cell death induced by nab-PTX (Fig. 1H and I).

Since PTX is responsible for the killing effect of nab-PTX [15], we also examined the correlation between LKB1 status and PTX in NSCLC cells. Similar to the observation of nab-PTX, LKB1 deficiency enhanced PTX-induced cell death in H1299 cells (Fig. S1A), while the reconstitution of WT-LKB1 impaired its killing effect in A549 cells (Fig. S1B). Given that PTX can induce several types of cell death under distinct circumstances [34–37], we further explored the type of cell death induced by nab-PTX in NSCLC cells. As showed in Figs. S1C and S1D, Z-VAD-FMK (a pan-caspase inhibitor), but not ferrostatin-1 (Fer-1, a ferroptosis inhibitor) and GSK872 (a necroptosis inhibitor), significantly

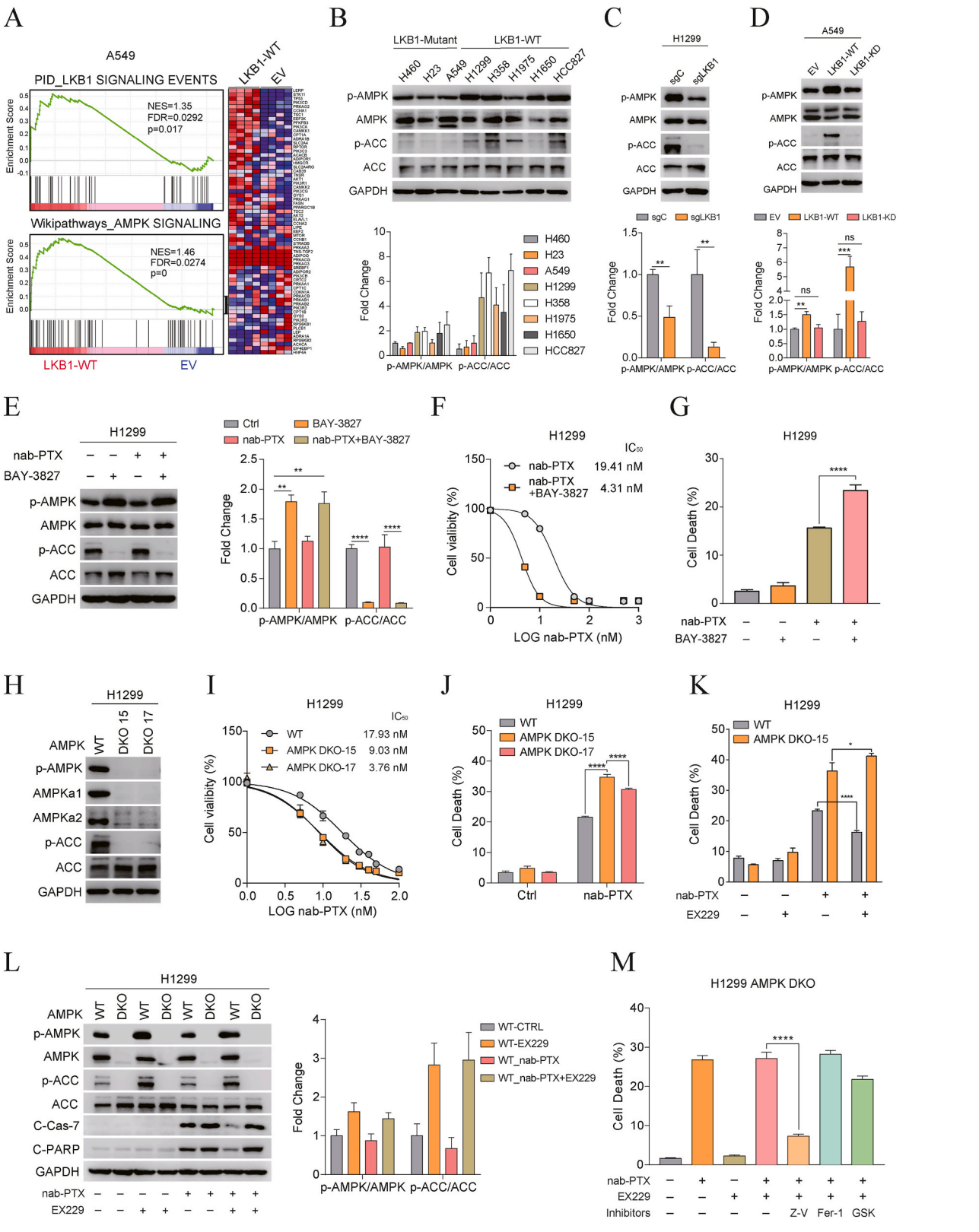

(caption on next page)

Fig. 3. AMPK inactivation sensitizes cells to apoptotic cell death induced by nab-PTX.
A. Gene set enrichment analysis (GSEA) using the Pathway Interaction Databases (PID) and Wikipathways database focusing on LKB1 signaling and AMPK signaling gene sets, respectively. FDR, false discovery rate; NES, normalized enrichment score. **B**. An immunoblot showing the levels of AMPK T172 phosphorylation, AMPK, ACC S79 phosphorylation and ACC in various NSCLC cell lines. **C-D**. An immunoblot showing the levels of AMPK T172 phosphorylation, AMPK, ACC S79 phosphorylation and ACC in indicated H1299 cells (**C**) and in indicates A549 cells (**D**). **E**. An immunoblot showing the levels of AMPK T172 phosphorylation, AMPK, ACC S79 phosphorylation and ACC in H1299 cells treated with 50 nM nab-PTX combined with or without 10 μM BAY-3827 for 24 h. **F**. Cell viability measurement in H1299 cells treated with indicated concentrations of nab-PTX combined with or without 10 μM BAY-3827 for 72 h. **G**. Cell death measurement in H1299 cells treated with 50 nM nab-PTX combined with or without 10 μM BAY-3827 for 36 h. **H**. An immunoblot indicating the loss of *AMPKα1/α2* in *AMPK* DKO H1299 cell lines generated using CRISPR–Cas9 system. **I**. Cell viability measurement in *AMPK* WT and DKO H1299 cells treated with indicated concentrations of nab-PTX for 72 h. **J**. Cell death measurement in *AMPK* WT and DKO H1299 cells treated with 50 nM nab-PTX for 36 h. **K**. Cell death measurement in *AMPK* WT and DKO H1299 cells treated with 50 nM nab-PTX with or without 40 μM EX229 for 36 h. **L**. Immunoblot showing the levels of AMPK T172 phosphorylation, AMPK, ACC S79 phosphorylation, ACC, cleaved-caspase 7 (C-Cas-7), and cleaved PARP (C-PARP) in *AMPK* WT and DKO H1299 cells treated as in **K**. **M**. Cell death measurement in *AMPK* DKO H1299 cells treated with 50 nM nab-PTX, 40 μM EX229, and various cell death inhibitors. Z-V, 20 μM Z-VAD-FMK; Fer-1, 5 μM ferrostatin-1; GSK, 20 μM GSK-872. sgC, sgCtrl; EV, empty vector; WT, wild-type. ns, not statistically significant; ****$p < 0.0001$. The mean ± s.d. is shown as $n \geq 3$ independent experiments. Statistical analyses were performed using unpaired two-tailed t-tests.

inhibited cell death induced by nab-PTX in both H1299 and A549 cells, indicating that nab-PTX induced apoptotic cell death in NSCLC cells. Meanwhile, we found that the addition of Z-VAD-FMK could also reduce the cell death induced by nab-PTX in *LKB1* knockout (KO) H1299 cells (Fig. 1J), accompanied by the downregulation of cleaved-caspase 7 level (Fig. S1E). Similar observations were made in A549 cells (Fig. 1K, Fig. S1F), suggesting that LKB1 status does not alter the type of cell death induced by nab-PTX. Finally, we tested whether LKB1 impairs the potency of nab-PTX *in vivo* using a nude mouse xenograft model. The results showed that nab-PTX displayed a stronger repression effect in the growth of *LKB1*-KO H1299 xenografts (Fig. 1L and M). Consistently, overexpression of LKB1 impaired the efficacy of nab-PTX in the growth suppression of A549 xenografts (Fig. 1N and O). Taken together, these data suggest that LKB1 impairs the therapeutic potential of nab-PTX in NSCLC by protecting against cell death induced by nab-PTX.

3.2. LKB1 does not affect the uptake of nab-PTX and its canonical pharmacological effects

An earlier report showed that the higher susceptibility of *Kras*-mutant cells to nab-PTX is due to the enhanced uptake of nab-PTX [33]. To explore whether LKB1 could also affect the uptake of nab-PTX in NSCLC cells, we performed liquid chromatography with tandem mass spectrometry (LC-MS/MS) to directly detect the intracellular concentration of PTX. The results showed that neither the deletion of *LKB1* in H1299 cells nor the overexpression of WT-LKB1 in A549 cells altered the intracellular concentration of nab-PTX, compared to their respective parental cells (Fig. 2A and B). Thus, our data indicated that LKB1 status has no direct role in regulating the uptake of nab-PTX. It is well known that the pharmacologic activity of PTX is via its direct binding to β-tubulin to promote the polymerization of microtubule, then leading to the stabilization and dysfunction of microtubule and subsequent cell cycle arrest at G2/M phase [38]. To investigate whether LKB1 can affect the pharmacological effects of nab-PTX, we detected changes in microtubules and found that LKB1 status did not significantly alter the dynamics of microtubules induced by nab-PTX (Fig. 2C and D). A cell cycle assay was also conducted to explore whether LKB1 impaired cell cycle profiles following treatment with nab-PTX. The results showed that nab-PTX induced a striking G2/M phase arrest in both H1299 and A549 cells in a dose-dependent manner (Fig. 2E). However, no significant change in cell cycle distribution was observed after the deletion of *LKB1* in H1299 cells or after the overexpression of LKB1 in A549 cells (Fig. 2F and G). Together, these data suggest that LKB1 status does not affect the cellular uptake and the canonical pharmacological actions of nab-PTX.

3.3. AMPK inactivation sensitizes cells to apoptotic cell death induced by nab-PTX in LKB1-WT NSCLC

To determine the mechanisms by which LKB1 impairs the efficacy of nab-PTX, RNA sequencing was performed to examine the changes in gene expression profiles after genetic alteration of *LKB1* in H1299 and A549 cells. By employing differentially expressed genes (DEGs) analysis, we observed that the overexpression of WT-LKB1 significantly upregulated 397 genes and downregulated 226 genes in A549 cells (Fig. S2A). Subsequently, we executed Hallmark-pathway enrichment analysis, and the top 10 gene sets were screened out, including epithelial mesenchymal transition, TGFβ signaling and hypoxia signialing (EMT), (Fig. S2B). We found that these screened pathways mostly require AMPK, which is a primary downstream substrate of LKB1 and plays a critical role in metabolism and cell death [24,39,40]. Therefore, we conducted gene set enrichment analysis (GSEA) and found that the overexpression of LKB1 in A549 cells indeed significantly activated AMPK signaling (Fig. 3A). In contrast, the deletion of *LKB1* impaired AMPK signaling in H1299 cells (Fig. S2C). Similar observations were obtained in H1650 cells, whose gene expression profiles (GSE69747) were acquired from GEO database (Fig. S2D). To further verify the results from the bioinformatics analyses, we directly measured the level of AMPK activation in a panel of NSCLC cell lines by immunoblotting. Consistently, higher levels of phosphorylation of AMPK in the T172 residue (*p*-AMPK) and ACC in the S79 residue (*p*-ACC) were found in the NSCLC cell lines with WT-*LKB1* in comparison to the cell lines with mutant *LKB1* (Fig. 3B). Furthermore, the deletion of *LKB1* strikingly reduced *p*-AMPK and *p*-ACC in H1299 cells (Fig. 3C), whereas the overexpression of WT-LKB1, but not the KD form, dramatically upregulated *p*-AMPK and *p*-ACC in A549 cells (Fig. 3D).

To explore whether AMPK is involved in the nab-PTX resistance induced by LKB1 in NSCLC, we firstly treated the cells with nab-PTX combined with or without BAY-3827, a specific and potent AMPK inhibitor [41,42]. Reduced levels of *p*-ACC upon treatment with BAY-3827 indicated the efficient inhibition of AMPK (Fig. 3E). Notably, the pharmacological inhibition of AMPK by BAY-3827 significantly enhanced the cytotoxicity of nab-PTX in H1299 (Fig. 3F and G) and H358 cells (Figs. S2E and S2F). Moreover, using CRISPR/Cas9 technology, we established an *AMPKα1/AMPKα2* double knockout (*AMPK*-DKO) in H1299 cells and found that the deletion of *AMPK* dramatically sensitized the cells to the treatment of nab-PTX (Fig. 3H–J). To further verify the role of AMPK, we tested the effect of EX229, an allosteric AMPK activator, and found that the addition of EX229 significantly protected cells from cell death induced by nab-PTX only in *AMPK*-WT cells, but not in *AMPK*-DKO cells (Fig. 3K and L). Z-VAD-FMK, a general caspase inhibitor, significantly reduced the cell death induced by nab-PTX in *AMPK*-DKO cells (Fig. 3M). Notably, a relatively lower *p*-AMPK level in H1975 cells could be observed, which is likely the cause for its sensitivity to nab-PTX in comparison to other LKB1-WT NSCLC cell lines (Fig. 1B, C, 3B). Taken together, these results indicate that AMPK activation downstream of LKB1 exerts protective effect, and AMPK inactivation sensitizes cells to apoptotic cell death induced by nab-PTX.

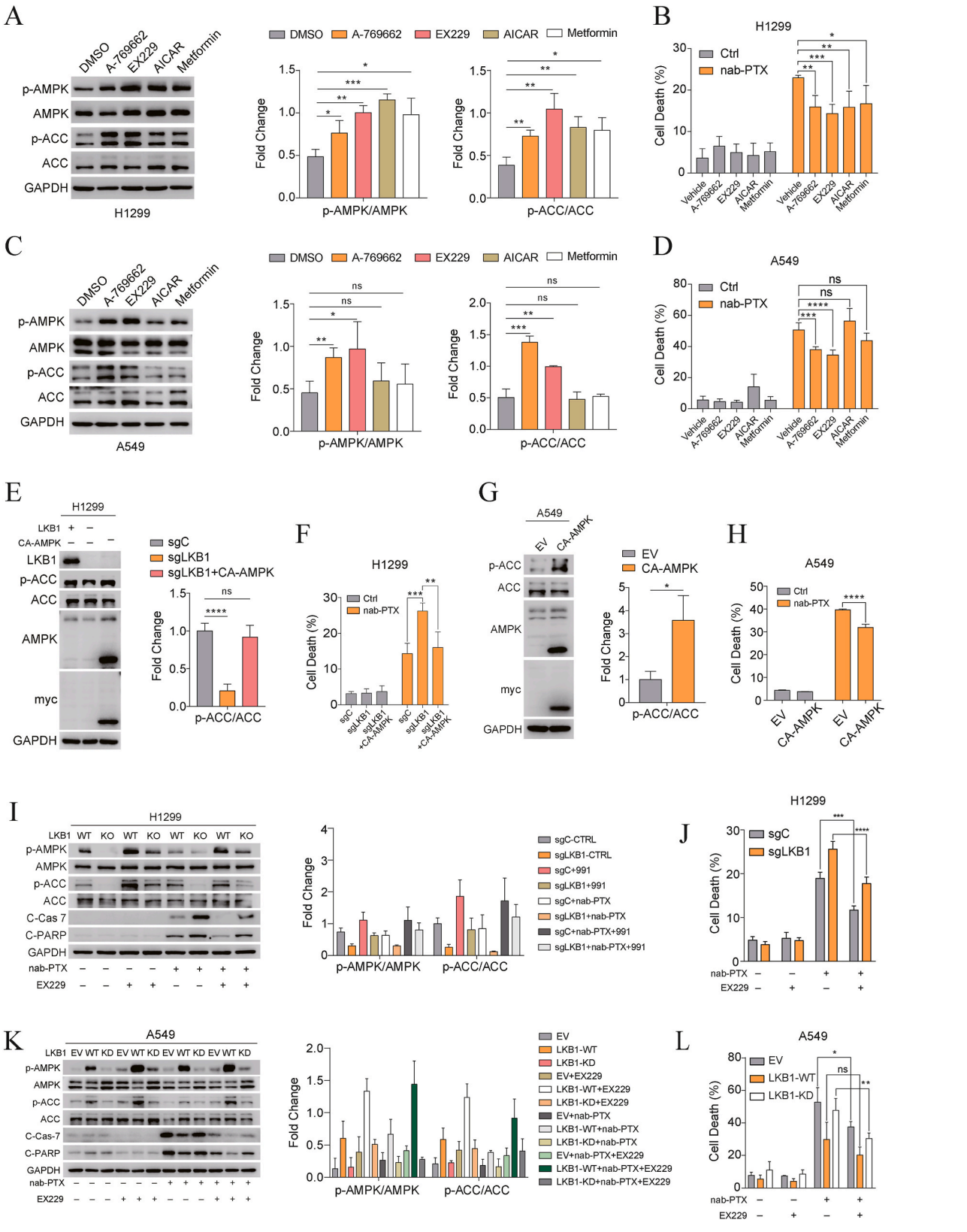

(caption on next page)

Fig. 4. LKB1 inhibits nab-PTX induced apoptotic cell death through AMPK activation.
A. An immunoblot showing the levels of AMPK T172 phosphorylation, AMPK, ACC S79 phosphorylation, ACC in H1299 cells treated with 200 μM A-769662, 40 μM EX229, 200 μM AICAR and 1 mM Metformin for 24 h, respectively. **B**. Cell death measurement in H1299 cells treated with 50 nM nab-PTX combined with or without indicated AMPK activators for 36 h. **C**. An immunoblot showing the levels of AMPK T172 phosphorylation, AMPK, ACC S79 phosphorylation, ACC in A549 cells treated as in **A**. **D**. Cell death measurement in A549 cells treated with 50 nM nab-PTX combined with or without indicated AMPK activators for 36 h. **E**. An immunoblot showing the expression of CA-AMPK and ACC S79 phosphorylation in *LKB1* KO H1299 cells. **F**. Cell death measurement in indicated H1299 cells upon the treatment of 50 nM nab-PTX for 36 h. **G**. An immunoblot showing the expression of CA-AMPK and ACC S79 phosphorylation in A549 cells. **H**. Cell death measurement in indicated A549 cells treated with 50 nM nab-PTX for 36 h. **I**. An immunoblot showing AMPK T172 phosphorylation, AMPK, ACC S79 phosphorylation, ACC, C-Cas-7, and C-PARP in indicated H1299 cells treated with 50 nM nab-PTX combined with or without 40 μM EX229 for 24 h. **J**. Cell death measurement in indicated H1299 cells treated with 50 nM nab-PTX combined with or without 40 μM EX229 for 36 h. **K**. An immunoblot showing AMPK T172 phosphorylation, AMPK, ACC S79 phosphorylation, ACC, C-Cas-7, and C-PARP in indicated A549 cells treated as in **I**. **L**. Cell death measurement in indicated A549 cells treated as in **J**. C-Cas-7, cleaved-caspase 7; C-PARP, cleaved-PARP. sgC, sgCtrl; EV, empty vector; WT, wide type; KD, kinase dead. ns, no statistical significance; *$p < 0.05$; **$p < 0.01$; ***$p < 0.001$; ****$p < 0.0001$. The mean ± s.d. are shown; $n \geq 3$ independent experiments. Statistical analysis was performed using an unpaired, two-tailed *t*-test.

3.4. *LKB1 impairs nab-PTX-induced apoptotic cell death through AMPK activation*

To further verify whether AMPK activation plays a causal role in determining the sensitivity of nab-PTX downstream of LKB1, we tested a series of AMPK activators, including AICAR, metformin, A-769662 and EX229. Based on the mechanism by which they activate AMPK, these activators can be divided into two groups: AICAR and metformin are LKB1-dependent and regulated by the intracellular AMP/ATP ratio, while A-769662 and EX229 are LKB1-independent and act allosterically by binding to the β-subunit of AMPK [43]. In H1299 cells with WT-*LKB1*, both LKB-dependent and LKB1-independent AMPK activators significantly enhanced the activation of AMPK (Fig. 4A) and reduced the cell death induced by nab-PTX (Fig. 4B). As expected, in A549 cells with mutated *LKB1*, only LKB1-independent AMPK activators (A-769662 and EX229) activated AMPK (Fig. 4C) and displayed a protective effect (Fig. 4D). Moreover, we reconstituted constitutively activated (CA) AMPK (amino acids 1–312 of AMPKα1) in *LKB1* KO H1299 cells and found that overexpression of CA-AMPK moderately increased the phosphorylation of ACC (Fig. 4E) and partially reduced the cell death induced by nab-PTX (Fig. 4F). A similar function of CA-AMPK was observed in A549 cells in which *LKB1* is mutant (Fig. 4G and H). Moreover, the deletion of *LKB1* in H1299 cells did not alter the effects of EX229, a LKB1-independent AMPK activator, on AMPK activation and apoptotic cell death induced by nab-PTX (Fig. 4I and J). Similarly, the protective effect of EX229 against nab-PTX-induced cell death was observed in A549 cells regardless of the status of LKB1 (Fig. 4K and L). Above all, these data indicate that LKB1 inhibits nab-PTX-induced apoptotic cell death through AMPK activation.

3.5. *Activation of the LKB1-AMPK signaling pathway inhibits nab-PTX-induced apoptosis by impairing ROS production*

We next sought to study the underlying mechanism(s) by which the LKB1-AMPK signaling pathway leads to the resistance to nab-PTX. Given that AMPK can reduce reactive oxygen species (ROS) under several stress conditions [44–46] and ROS is one of the key effectors of the anticancer efficacy of PTX [47,48], we deduced that the activation of AMPK can reduce the ROS level induced by nab-PTX, which partially protects the cells from the apoptotic cell death. To test this hypothesis, we first detected the ROS level in cells treated with nab-PTX. As showed in Fig. 5A–B, nab-PTX significantly increased the ROS level in A549 cells. To confirm the proapoptotic role of ROS, N-Acetylcysteine (NAC), a well-known and effective ROS scavenger [49], was applied for the experiment. As expected, NAC significantly reduced the ROS level (Fig. 5C and D) and repressed the apoptotic cell death (Fig. 5E and F) induced by nab-PTX in A549 cells. Moreover, the allosteric activator of AMPK, EX229, significantly reduced the ROS level induced by nab-PTX in A549 cells (Fig. 5G and H). In addition, overexpression of WT-LKB1 in A549 cells led to lower level of ROS production induced by nab-PTX (Fig. 5I and J), and consistently NAC displayed a weaker inhibitory effect on ROS level in *LKB1*-WT A549 cells (Fig. 5I and J). Correspondingly, NAC exhibited a relatively weaker protective effect against cell death induced by nab-PTX in *LKB1*-WT A549 cells. (Fig. 5K and L). Conversely, BAY-3827, an AMPK inhibitor, significantly increased the ROS level (Fig. 5M and N) and promoted the apoptotic cell death induced by nab-PTX (Fig. 5O and P) in *LKB1*-WT A549 cells. Taken together, our data suggests that the activation of LKB1-AMPK signaling pathway inhibits apoptosis induced by nab-PTX through the regulation of ROS production and oxidative stress.

3.6. *Upregulation of the LKB1-AMPK-SLC7A11-GSH pathway mediates nab-PTX resistance in LKB1-WT NSCLC cells*

To further explore the mechanism by which LKB1-AMPK activation inhibits the production of ROS and cell death induced by nab-PTX, we first performed gene set enrichment analysis and found that the overexpression of WT LKB1 significantly enhanced the antioxidant signaling pathway in A549 cells (Fig. S3A). In contrast, the deletion of *LKB1* obviously impaired the antioxidant signaling in H1299 cells (Fig. S3B). Given that glutathione (GSH) is the major antioxidant to prevent cells from the damage of ROS [50], we next measured the level of intracellular GSH after the genetic alteration of *LKB1* in H1299 and A549 cells. Results showed that the deletion of *LKB1* significantly decreased the GSH level in H1299 cells (Fig. 6A), while the overexpression of WT LKB1 but not its kinase dead form increased the GSH level in A549 cells (Fig. 6B). To verify the role of GSH in the cell death induced by nab-PTX, we tested the effect of DL-Buthionine-(S,R)-sulfoximine hydrochloride (BSO), a potent inhibitor of γ-glutamylcysteine synthetase (GCS, the first enzyme of the cellular GSH biosynthetic pathway). As expected, a significant reduction of cellular GSH level was observed upon the treatment of BSO (Fig. 6C). Meanwhile, BSO strikingly enhanced cell death caused by nab-PTX in H1299 cells (Fig. 6D and E), demonstrating the important role of GSH in protecting the apoptotic cell death induced by nab-PTX.

We then tried to investigate the molecular mechanism by which LKB1 increases the cellular GSH level. It has been well established the intracellular GSH level is tightly regulated by a group of enzymes: SLC7A11, the transporter of cystine which is a substrate of GSH biosynthesis; γ-glutamylcysteine synthetase (GCS) and glutathione synthetase (GSS), who are responsible for the De novo synthesis of GSH; Glutathione peroxidase 4 (GPX4), which catalyzes GSH to glutathione disulfide (GSSG) and glutathione reductase (GR), which restores GSH by catalyzing the reverse reaction [51](Fig. 6F). In this study, we found that the deletion of *LKB1* significantly downregulated the mRNA level of SLC7A11 in H1299 cells (Fig. 6G) whereas overexpression of LKB1 increases its mRNA level in A549 cells (Fig. 6H). Furthermore, similar changes of SLC7A11 protein levels could also be observed in H1299 and A549 cells (Fig. 6I and J). Moreover, we found an obvious downregulation of SLC7A11 in *AMPK*-DKO cells compared to the *AMPK*-WT cells (Fig. 6K), suggesting the causal role of AMPK in regulation of SLC7A11 downstream of LKB1. Consistently, double knockout of *AMPK* significantly reduced the cellular GSH level (Fig. 6L). In addition, the

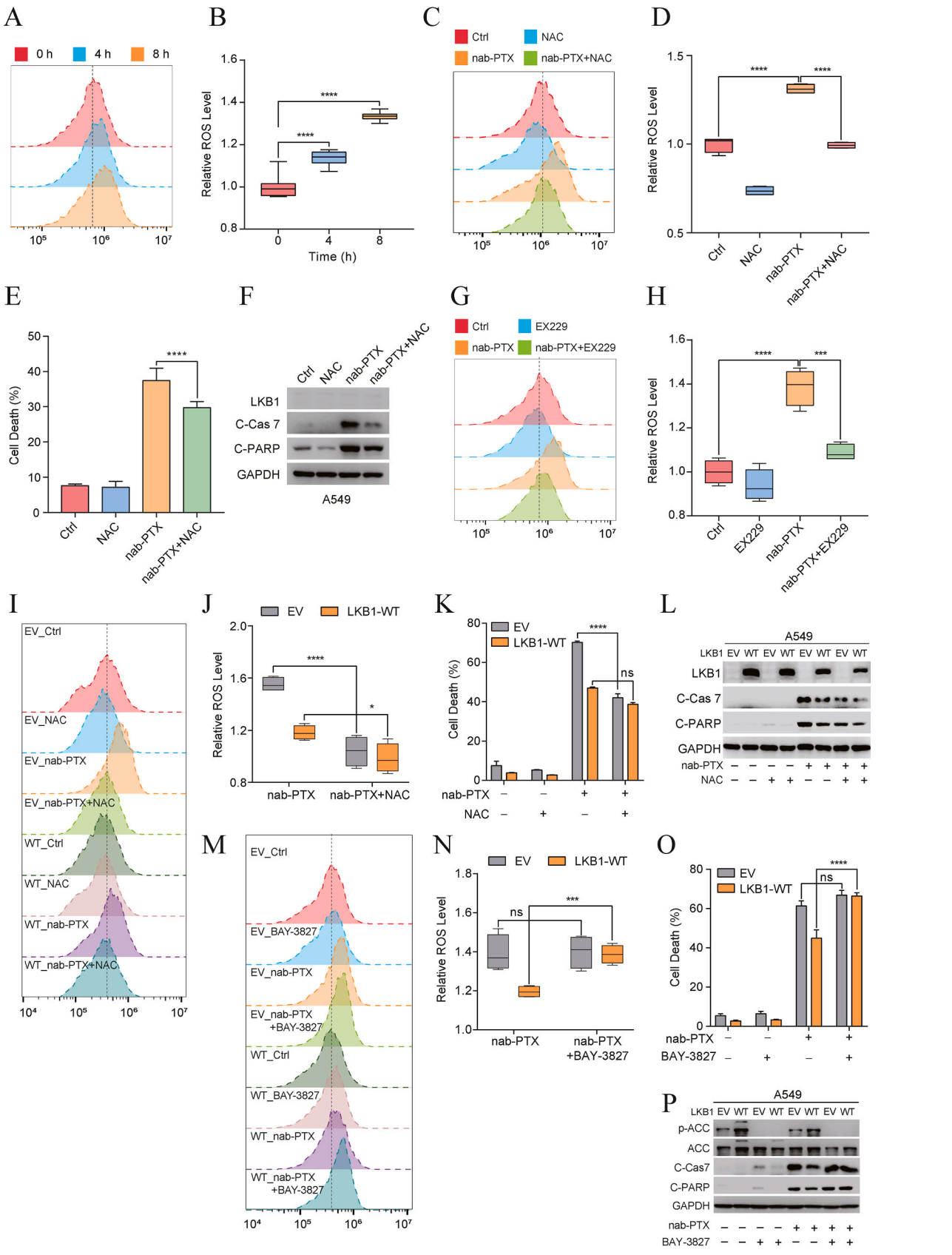

(caption on next page)

Fig. 5. Activation of the LKB1-AMPK signaling pathway inhibits nab-PTX induced apoptosis by impairing ROS production.
A. Representative images showing the production of ROS in A549 cells treated with 50 nM nab-PTX for indicated time point. **B**. ROS measurement in A549 cells treated as in **A**. **C**. Representative images showing the productions of ROS in A549 cells treated with 50 nM nab-PTX combined with or without 10 mM NAC for 4 h. **D**. ROS measurement in A549 cells treated as in **C**. **E**. Cell death measurement in A549 cells treated with 50 nM nab-PTX combined with or without 10 mM NAC for 36 h. **F**. An immunoblot showing the expression of C-Cas-7 and C-PARP in A549 cells treated with 50 nM nab-PTX combined with or without 10 mM NAC for 24 h. **G**. Representative images showing the productions of ROS in A549 cells treated with 50 nM nab-PTX combined with or without 40 μM EX229 for 4 h. **H**. ROS measurement in A549 cells treated as in **G**. **I**. Representative images showing the productions of ROS in indicated A549 cells treated with 50 nM nab-PTX combined with or without 10 mM NAC for 4 h. **J**. ROS measurement in indicated A549 cells treated as in **I**. **K**. Cell death measurement in indicated A549 cells treated with 50 nM nab-PTX combined with or without 10 mM NAC for 36 h. **L**. An immunoblot showing the expression of C-Cas-7 and C-PARP in indicated A549 cells treated with 50 nM nab-PTX combined with or without 10 mM NAC for 24 h. **M**. Representative images showing the productions of ROS in indicated A549 cells treated with 50 nM nab-PTX combined with or without 10 μM BAY-3827 for 4 h. **N**. ROS measurement in indicated A549 cells treated as in **M**. **O**. Cell death measurement in indicated A549 cells treated with 50 nM nab-PTX combined with or without 10 μM BAY-3827 for 36 h. **P**. An immunoblot showing the expression of C-Cas-7 and C-PARP in indicated A549 cells treated with 50 nM nab-PTX combined with or without 10 μM BAY-3827 for 24 h. C-Cas-7, cleaved-caspase 7; C-PARP, cleaved-PARP; EV, empty vector; WT, wide type. ns, no statistical significance; *$p < 0.05$; ****$p < 0.0001$. The mean ± s.d. are shown; $n \geq 3$ independent experiments. Statistical analysis was performed using an unpaired, two-tailed *t*-test.

overexpression of a constitutively active form of AMPK (CA-AMPK) apparently restored the expression of SLC7A11 and increased the cellular GSH level in *LKB1* KO H1299 cells (Fig. 6M and N). In addition to the genetic approaches, we also used a pharmacological reagent, EX229, an LKB1-independent AMPK activator, and found that EX229 dramatically upregulated the expression of SLC7A11 and increased the cellular GSH level both in *LKB1* WT and *LKB1* KO H1299 cells (Fig. 6O and P). Interestingly, only the LKB1-independent AMPK activators (A-769662 and EX229) but not the LKB1-dependent AMPK activators displayed a potent effect on the upregulation of SLC7A11 in A549 cells (Fig. S3C), further demonstrating the critical role of LKB1-AMPK signaling in determining the cell death induced by nab-PTX.

Based on the above results, we reasoned that SLC7A11 might play a positive role in the primary resistance of nab-PTX in *LKB1*-WT NSCLC. To verify our hypothesis, we knocked down (KD) *SLC7A11* in H1299 cells (Fig. 6Q) and found dramatic reduction of cellular GST level (Fig. 6R) in cells with KD of *SLC7A11*. As expected, a higher ROS level and more cell death could be observed in *SLC7A11* KD H1299 cells after the treatment of nab-PTX (Fig. 6S–U). Meanwhile, we also overexpressed SLC7A11 in *LKB1* KO H1299 cells (Fig. 6V). The overexpression of SLC7A11 significantly restored the cellular GST level (Fig. 6W), reduced the ROS accumulation (Fig. 6X), and impaired the cell death induced by nab-PTX (Fig. 6Y and Z). Similar effects of SLC7A11-overexpression could also be observed in A549 cells (Figs. S3D–F).

Taken together, data from this part of our study suggest that the activation of LKB1-AMPK signaling pathway increases cellular GSH level by promoting SLC7A11 expression, which attenuates the efficacy of nab-PTX through the regulation of ROS production and cell death.

3.7. Inhibition of AMPK sensitizes LKB1-WT NSCLC to nab-PTX in vivo

To evaluate whether the inhibition of AMPK can promote the therapeutic potency of nab-PTX *in vivo*, we established nude mice xenografts using H1299 and H358 cells, both with WT-*LKB1*, in which the animals were treated with nab-PTX with or without the AMPK inhibitor BAY-3827. To visualize tumor growth *in vivo*, lentiviruses expressing EGFP were infected to these cells before subcutaneous injection into the mice. Combined treatment with nab-PTX and BAY-3827 displayed a stronger therapeutic effect as measured by tumor growth and tumor volume in H1299-derived xenografts (Fig. 7A–C). Similarly, the combination treatment of nab-PTX and BAY-3827 also showed a better therapeutic effect in H358-derived xenografts than nab-PTX alone (Fig. 7D–F). The combined effect of nab-PTX and BAY-3827 was recapitulated by immunohistochemistry (IHC) staining analysis of the xenograft tumors, in which *p*-ACC was abrogated by BAY-3827 in both H1299- and H358-derived xenografts (Fig. 7G -J). BAY-3827 also enhanced the efficacy of nab-PTX in inhibiting tumor cell proliferation and increasing tumor cell death, as quantified by Ki-67 and p-H2A.X staining, respectively (Fig. 7G-J). Taken together, these data suggest that AMPK inhibition sensitizes *LKB1*-WT NSCLC to nab-PTX.

4. Discussion

Chemotherapy is usually considered as a non-targeted treatment, as chemotherapeutic agents usually act via direct inhibition of DNA synthesis or causing damage to DNA and proteins [52]. Conceptually, one chemotherapeutic drug should be available for the treatment of all kinds of cancer. However, the application of a chemotherapeutic drug is usually limited to not more than 5 types of cancer. For instance, nab-PTX has been approved by the FDA for the treatment of metastatic breast cancer, locally advanced or metastatic NSCLC and advanced pancreatic cancer [16]. Similarly, cisplatin, another well-known chemotherapeutic drug, is approved for the treatment of advanced ovarian cancer, testicular cancer, and bladder cancer [53,54]. Therefore, it remains a challenge whether a chemotherapeutic drug such as nab-PTX can also be targeted to a specific group of cancer patients with a specific genetic background. In this study, we found that NSCLC with mutant-*LKB1* is more sensitive to nab-PTX in comparison to those NSCLC with WT-*LKB1*. Mechanistically, LKB1 status does not alter the intracellular concentration of nab-PTX or affect its canonical pharmacological action in promoting microtubule polymerization. The deficiency of AMPK activation reduces the expression of SLC7A11 and leads to a lower cellular GSH level, which sensitizes *LKB1*-mutant NSCLC to oxidative stress and cell death induced by nab-PTX. On the other hand, genetic or pharmacological inhibition of AMPK is capable of sensitizing *LKB1*-WT NSCLC to nab-PTX (Fig. 8). Therefore, our data reveal a novel role of LKB1-AMPK-SLC7A11-GSH signaling pathway in the primary resistance to nab-PTX, and provide a therapeutic strategy for the treatment of *LKB1*-WT NSCLC by targeting the LKB1-AMPK-SLC7A11 pathway.

An earlier report by Li R et al. found that nab-PTX has higher selectivity towards murine *Kras*-mutant NSCLC via increased uptake of nab-PTX, a process associated with enhanced level of AMPK activation [33]. As LKB1 is the key upstream kinase of AMPK, we attempted to explore whether the LKB1-AMPK pathway would also affect the cellular uptake of nab-PTX in NSCLC. Intriguingly, we found that the LKB1-AMPK status has no evident effect on the cellular uptake of nab-PTX, neither alters its effects on microtubule and cell cycle. We believe that this discrepancy may be caused by different contexts. Actually, a recent study has pointed out the distinct role of LKB1 in the development of human and murine NSCLC: murine NSCLC cells with mutated *LKB1* exhibited an advantage in tumor growth *in vivo*, whereas mutation of *LKB1* in human NSCLC cells impaired tumor growth in a mouse xenograft model [55].

In addition to AMPK, other 12 AMPK-related kinase (MARK1, MARK2, MARK3, MARK4, SAD-A, SAD-B, QIK, QSK, NUAK1, NUAK2, SIK, and SNRK) that contain the LXT motif in their activation loop have also been identified as the substrates of LKB1 [56]. Among them, microtubule affinity regulating kinase (MARK) 1/2/3/4 and synapses of amphids defective (SAD)-A/B have been reported to regulate tubulin polymerization through phosphorylation of microtubule-associated proteins (MAPs), such as Tau, MAP2, and MAP4 [57]. Therefore, LKB1

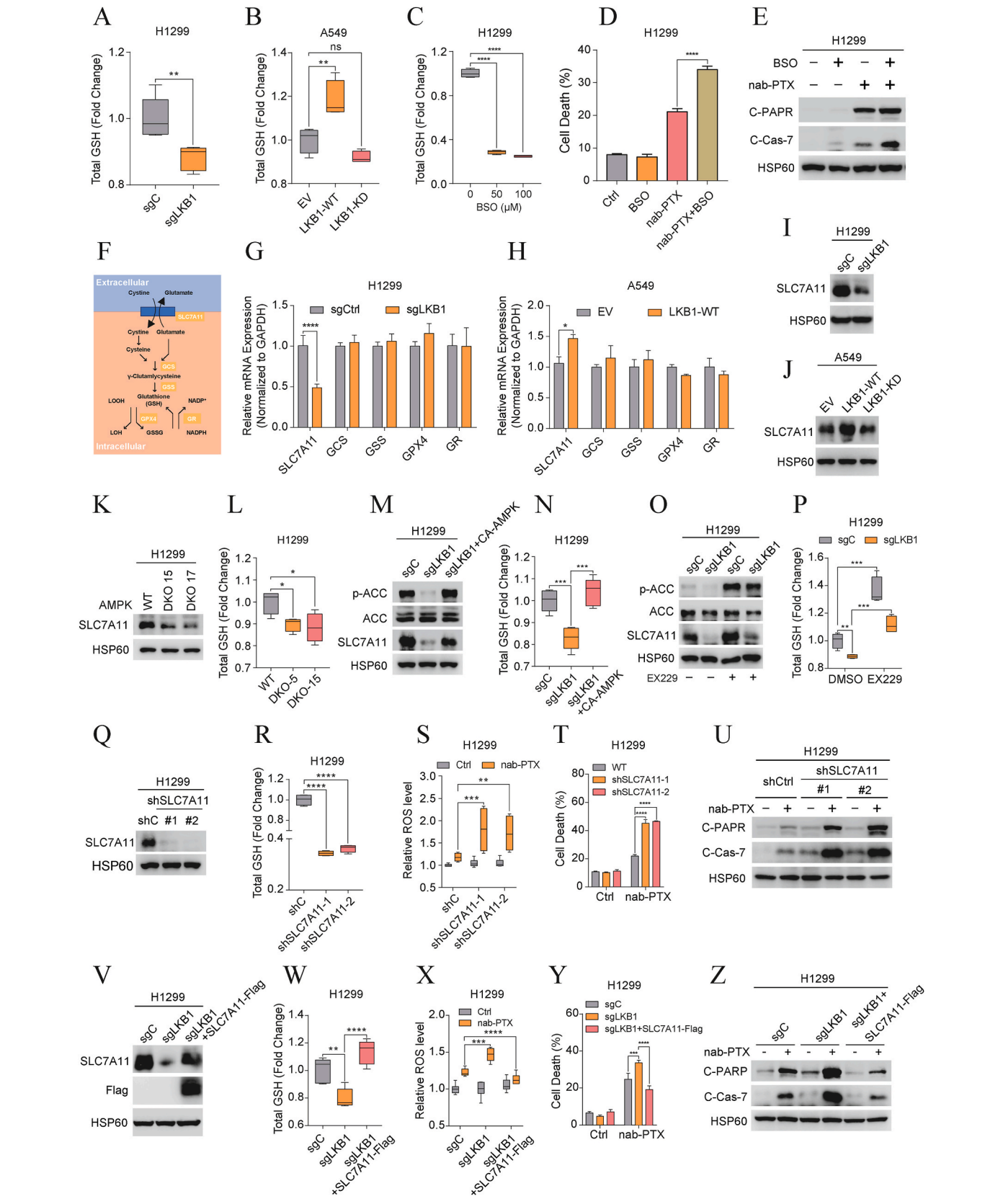

(caption on next page)

Fig. 6. Upregulation of the LKB1-AMPK-SLC7A11-GSH pathway mediates nab-PTX resistance in *LKB1*-WT NSCLC cells.
A-B. Cellular GSH measurement in indicated H1299 (**A**) and A549 (**B**) cells. **C**. Cellular GSH measurement in H1299 cells treated with indicated concentration of BSO for 24 h. **D**. Cell death measurement in H1299 cells treated with 50 nM nab-PTX in combination with or without 50 μM BSO for 36 h. **E**. An immunoblot showing the expression of C-Cas-7 and C-PARP in H1299 cells treated with 50 nM nab-PTX combined with or without 50 μM BSO for 24 h. **F**. Graphical summary of GSH metabolism. **G-H**. mRNA levels of GSH metabolism-related genes in indicated H1299 (**G**) and A549 (**H**) cells. **I-J**. An immunoblot showing the expression of SLC7A11 in indicated H1299 (**I**) and A549 (**J**) cells. **K**. An immunoblot showing the expression of SLC7A11 in indicated H1299 cells. **L**. Cellular GSH measurement in indicated H1299 cells. **M**. An immunoblot showing the ACC S79 phosphorylation and the expression of SLC7A11 in indicated H1299 cells. **N**. Cellular GSH measurement in indicated H1299 cells. **O**. An immunoblot showing the ACC S79 phosphorylation and the expression of SLC7A11 in indicated H1299 cells treated with or without 40 μM EX229 for 24 h. **P**. Cellular GSH measurement in indicated H1299 cells treated with or without 40 μM EX229 for 24 h. **Q**. An immunoblot showing the downregulation of SLC7A11 in *SLC7A11-knockdown* H1299 cells. **R**. Cellular GSH measurement in indicated H1299 cells. **S-T**. ROS measurement (**S**) and cell death measurement (**T**) in indicated H1299 cells treated with 50 nM nab-PTX for 4 h or 36 h, respectively. **U**. An immunoblot showing the expression of C-Cas-7 and C-PARP in indicated H1299 cells treated with 50 nM nab-PTX for 24 h. **V**. An immunoblot showing the expression of SLC7A11 in indicated H1299 cells. **W**. Cellular GSH measurement in indicated H1299 cells. **X–Y**. ROS measurement (**X**) and cell death measurement (**Y**) in indicated H1299 cells treated with 50 nM nab-PTX for 4 h or 36 h, respectively. **Z**. An immunoblot showing the expression of C-Cas-7 and C-PARP in indicated H1299 cells treated with 50 nM nab-PTX for 24 h. C-Cas-7, cleaved-caspase 7; C-PARP, cleaved-PARP. EV, empty vector; WT, wide type. ns, no statistical significance; *$p < 0.05$; **$p < 0.01$; ***$p < 0.001$; ****$p < 0.0001$. The mean ± s.d. are shown; $n \geq 3$ independent experiments. Statistical analysis was performed using an unpaired, two-tailed *t*-test.

may play a regulatory role in microtubule dynamics. Recently, Kojima et al. reported that LKB1 can directly phosphorylate and activate MARK2, which in turn phosphorylates the microtubule-associated protein Tau and suppresses tubulin polymerization [58]. Meanwhile, Mian et al. also reported that the overexpression of LKB1 destabilizes microtubule in myoblast cells [59]. However, in our study, the LKB1 status does not show a dramatic effect on the changes of microtubule dynamics induced by nab-PTX, thus excluding the possibility that the high susceptibility of *LKB1*-mutant NSCLC cells to nab-PTX is caused by alterations in microtubule polymerization induced by nab-PTX in NSCLC cells.

At present, the relationship between ROS/oxidative stress and AMPK activation is intricate. From the perspective of the impact of ROS on AMPK, it seems that ROS play a dual role in AMPK activation. On one hand, ROS are usually considered as a trigger of AMPK signaling, because high level of ROS impairs mitochondrial function and increases the cellular AMP level, which subsequently promotes AMPK activation [60,61]. Meanwhile, it is also reported that the elevation of ROS can directly oxidize redox-sensitive cysteine residues on the α subunit of AMPK, leading to AMPK activation [62]. On the other hand, some studies demonstrated that ROS and oxidative stress impair AMPK activation via direct oxidation of its key residues or protein degradation [63,64]. It appears that the different effects of ROS/oxidative stress on AMPK activation may be due to the distinction in cellular contents, the amount of ROS and the types of ROS. Similarly, AMPK also plays a dual role in ROS/oxidative stress. Generally, the activation of AMPK is considered to compromise ROS/oxidative stress under different stress conditions [25,31,65,66]. However, some studies also reported that AMPK activity contributes to oxidative stress. For instance, Song et al., demonstrated that AMPK-mediated phosphorylation of BECN1 at Ser90/93/96 is necessary for the formation of BECN1-SLC7A11 complex, which promotes the lipid peroxidation upon the treatment of SLC7A11 inhibitors [67].

In this study, one important finding is that activated AMPK enhances the expression of SLC7A11. Recently, some studies reported that activated AMPK promotes SLC7A11 expression via phosphorylation and stabilization of NRF2 that is considered as a transcription factor of SLC7A11 [68,69]. Meanwhile, Wang et al. suggested that AMPK increases the protein stability of SLC7A11 by promoting its palmitoylation-mediated by ZDHHC8 [70]. More work is needed to establish the molecular mechanisms linking AMPK activation to SLC7A11 expression.

Based on the critical role of AMPK in various cellular processes including metabolism and cell death, significant progresses have been made in development of AMPK activators for treatment of obesity and diabetes [71]. In contrast, studies on developing AMPK inhibitors are stagnant. For a long period of time, Compound-C has been the only pharmacological inhibitor of AMPK for scientific research [41]. Recently, a novel and potent AMPK inhibitor, BAY-3827, has been developed [42], which displays a more than 100-fold inhibitory potency and a better selectivity to AMPK, in comparison to Compound-C [41]. In our study, the inhibitory effect of BAY-3827 on AMPK activity could be proved by the almost complete abolition of ACC S79 phosphorylation (Fig. 3E, Fig. S2E). Meanwhile, also it is intriguing to observe that there was a dramatic increase in AMPK T172 phosphorylation upon the treatment of BAY-3827 both in H1299 and H358 cells (Fig. 3E, Fig. S2E). A recent study also reported similar results induced by BAY-3827, due to the inhibitory effect of BAY-3827 on AMPK T172 dephosphorylation [41].

In summary, our study reveals a novel function of the LKB1-AMPK-SLC7A11-GSH signaling pathway in the regulation of primary resistance to nab-PTX in NSCLC and provides a rationale for the combination of nab-PTX with AMPK inhibitor in *LKB1*-WT NSCLC to achieve better therapeutic efficacy.

CRediT authorship contribution statement

Dade Rong: Data curation, Formal analysis, Investigation, Methodology, Project administration, Validation, Writing – original draft, Writing – review & editing. **Liangliang Gao:** Data curation, Investigation, Methodology. **Yiguan Chen:** Data curation, Investigation, Methodology. **Xiang-Zheng Gao:** Data curation, Investigation, Methodology. **Mingzhu Tang:** Investigation, Methodology.**Haimei Tang:** Investigation, Methodology. **Yuan Gao:** Investigation, Methodology. **Guang Lu:** Formal analysis, Writing – review & editing. **Zhi-Qiang Ling:** Methodology, Resources, Writing – review & editing. **Han-Ming Shen:** Methodology, Resources, Writing – review & editing.

Data access statement

All relevant data are within the paper and its Supporting Information files.

Funding

This project was supported by the following research grants to Shen HM from the University of Macau (CPG2023-0032-FHS, CPG2024-0035-FHS UM-MYRG2020-00022-FHS) and the Macau Science and Technology Development Fund (FDCT0078/2020/A2, 0031/2021/A1, FDCT0081/2022/AMJ, FDCT 0004/2021/AKP); National Key R&D Program of China (No. 2022YFE0205900) to Ling ZQ.

Declaration of competing interest

The authors declare no competing interests.

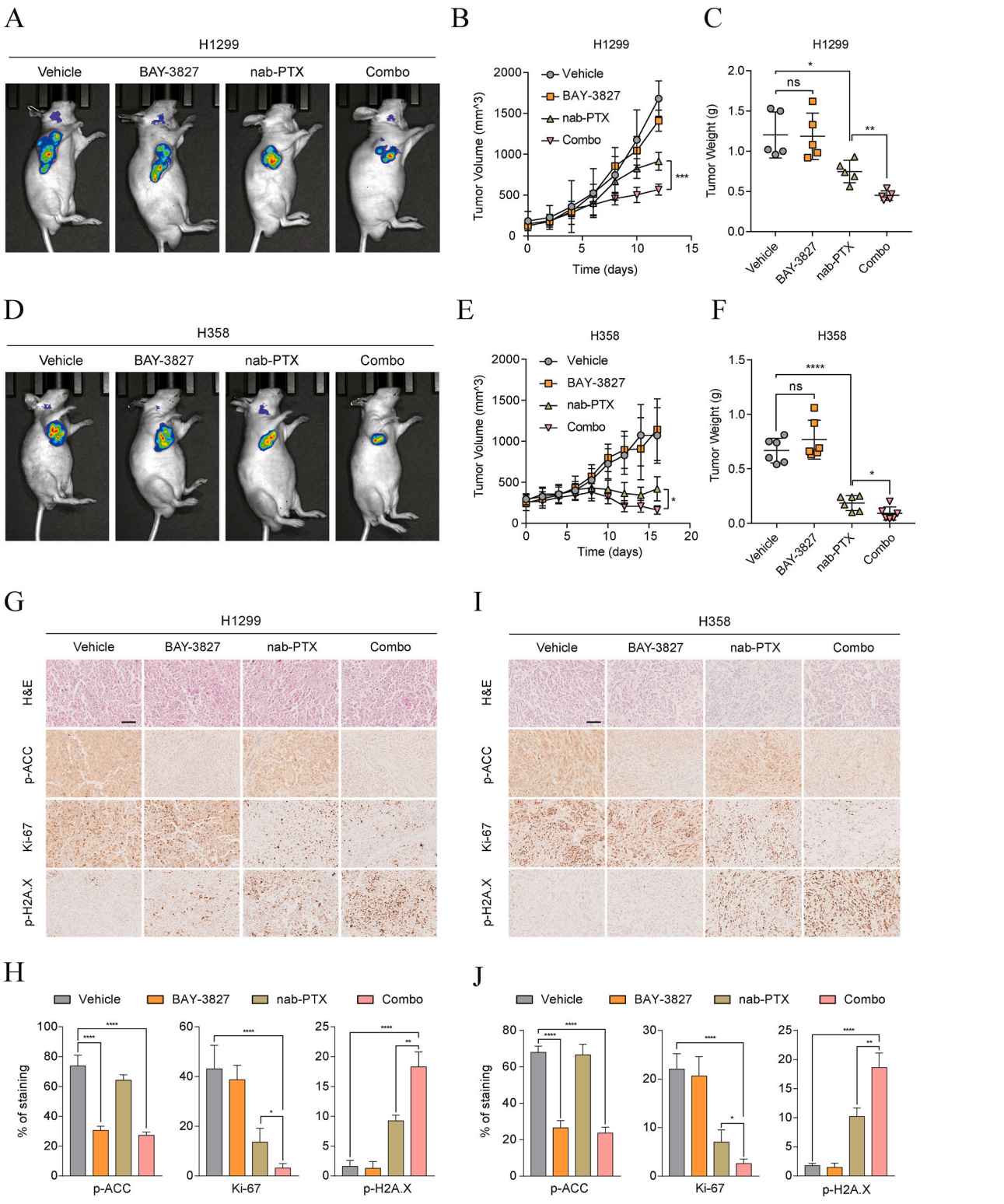

Fig. 7. Inhibition of AMPK increases therapeutic potential of nab-PTX in *LKB1*-WT NSCLC.
A. Representative images showing the tumor burden assessed by bioimaging in mice xenografted with H1299 cells upon the treatments of 10 mg/kg nab-PTX with or without 10 mg/kg BAY-3827. **B-C.** Tumor volume measurements over the course of the treatment (**B**) and final tumor weight measurement (**C**) in H1299-derived xenografts upon the treatment as in **A. D.** Representative images showing the tumor burden assessed by bioimaging in mice xenografted with H358 cells upon the treatments of 10 mg/kg nab-PTX with or without 10 mg/kg BAY-3827. **E-F.** Tumor volume measurements over the course of the treatment (**E**) and final tumor weight measurement (**F**) in H358-derived xenografts upon the treatment as in **D. G-H.** Representative immunohistological images showing the expression of ACC S79 phosphorylation, Ki-67, H2A.X S139 phosphorylation (**G**) and correlated quantifications (**H**) in H1299-derived xenografts upon the treatment as in **A. I-J.** Representative immunohistology images showing the expression of ACC S79 phosphorylation, Ki-67, H2A.X S139 phosphorylation (**I**) and correlated quantifications (**J**) in H358-derived xenografts upon the treatment as in **D.** Combo, nab-PTX combined with BAY-3827. Scale bar, 100 μM. ns, no statistical significance; *$p < 0.05$; **$p < 0.01$; ****$p < 0.0001$. The mean ± s.d. are shown; $n \geq 3$ independent experiments. Statistical analysis was performed using an unpaired, two-tailed *t*-test.

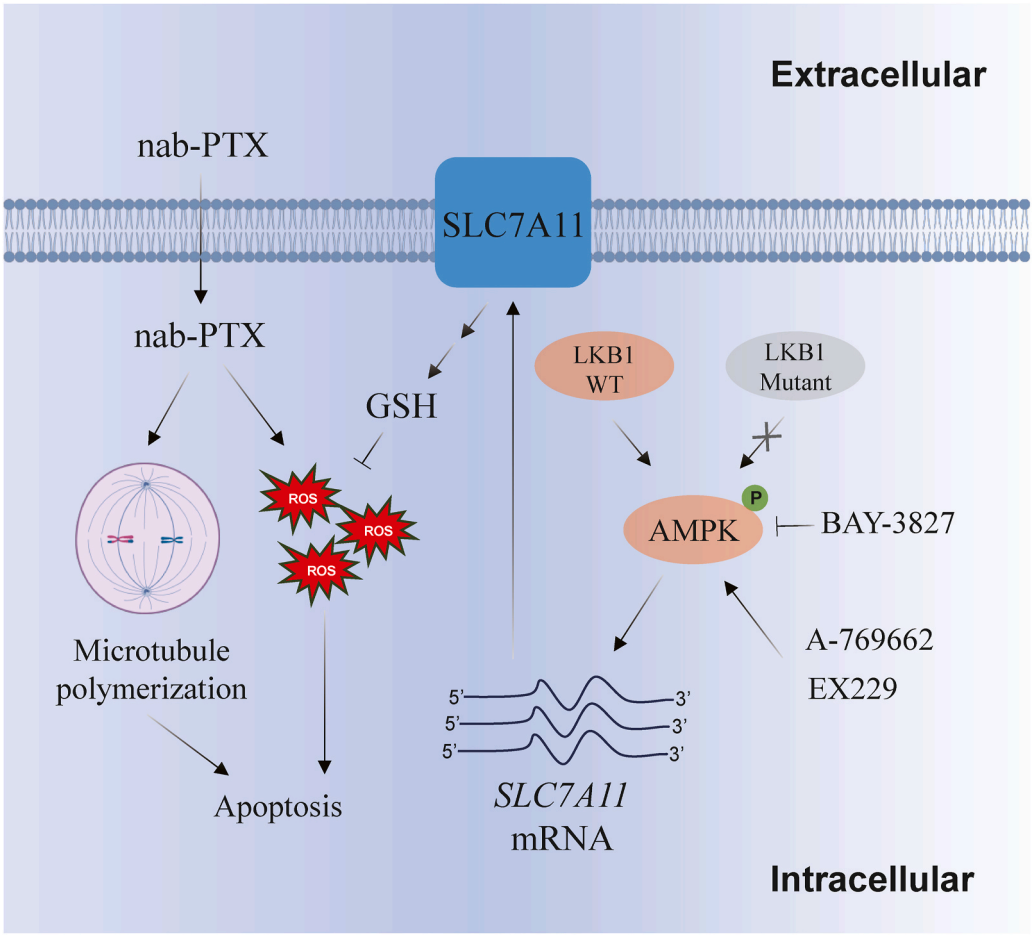

Fig. 8. Schematic model showing the mechanism by which LKB1 attenuates the efficacy of nab-PTX.
Activation of the LKB1-AMPK signaling pathway increases cellular GSH level by promoting the expression of SLC7A11, which impairs the therapeutic potential of nab-PTX for the reduction of ROS in *LKB1*-WT NSCLC cells. The combination treatment of AMPK inhibitor, BAY-3827, efficiently sensitized NSCLC cells to nab-PTX treatment both *in vitro* and *in vivo*.

Acknowledgements

Rong D, Gao L, Gao X, Chen Y, Tang M and Tang H were supported by UM Assistantship. Dr. Ke He from Guangdong Second People's Hospital provided us with albumin-bound paclitaxel (AiYue, Hengrui Pharmaceuticals Co., Ltd.). Dr. Xinhai Zhu from the Instrumental Analysis and Research Center, Sun Yat-sen University, provided technical services for intracellular drug concentration measurements. We thank the members of the Shen lab for their valuable discussions. We also thank the support from the Biological Imaging and Stem Cell Core, Animal Research Core, Genomics, Bioinformatics, and Single Cell Analysis Core at FHS of University of Macau to ensure efficient running of all experiments.

Abbreviations

(PTX) Paclitaxel
(nab-PTX) Albumin-bound Paclitaxel
(LKB1) Liver Kinase B1
(AMPK) AMP-activated protein kinase
(ACC) Acetyl-CoA carboxylase
(NAC) N-Acetylcysteine
(BSO) DL-Buthionine-(S,R)-sulfoximine hydrochloride
(GSH) Glutathione

Appendix A. Supplementary data

Supplementary data to this article can be found online at https://doi.org/10.1016/j.redox.2025.103567.

References

[1] R.L. Siegel, A.N. Giaquinto, A. Jemal, Cancer statistics, 2024, CA Cancer J. Clin. 74 (1) (2024) 12–49.
[2] A.A. Thai, B.J. Solomon, L.V. Sequist, J.F. Gainor, R.S. Heist, Lung cancer, Lancet 398 (10299) (2021) 535–554.
[3] G.S. Jones, D.R. Baldwin, Recent advances in the management of lung cancer, Clin. Med. 18 (Suppl 2) (2018) s41–s46.
[4] C. Zappa, S.A. Mousa, Non-small cell lung cancer: current treatment and future advances, Transl. Lung Cancer Res. 5 (3) (2016) 288–300.
[5] J. Rivera-Concepcion, D. Uprety, A.A. Adjei, Challenges in the Use of targeted therapies in non-small cell lung cancer, Cancer Res Treat 54 (2) (2022) 315–329.
[6] S.S. Bashraheel, A. Domling, S.K. Goda, Update on targeted cancer therapies, single or in combination, and their fine tuning for precision medicine, Biomed. Pharmacother. 125 (2020) 110009.
[7] C. Sordo-Bahamonde, S. Lorenzo-Herrero, A.P. Gonzalez-Rodriguez, A. Martínez-Pérez, J.P. Rodrigo, J.M. García-Pedrero, S. Gonzalez, Chemo-immunotherapy: a new Trend in cancer treatment, Cancers 15 (11) (2023).
[8] C. Grant, G. Hagopian, M. Nagasaka, Neoadjuvant therapy in non-small cell lung cancer, Crit. Rev. Oncol. Hematol. 190 (2023) 104080.
[9] M.H. Kim, S.H. Kim, M.K. Lee, J.S. Eom, Recent advances in adjuvant therapy for non-small-cell lung cancer, Tuberc. Respir. Dis. 87 (1) (2024) 31–39.
[10] J. Löwe, H. Li, K.H. Downing, E. Nogales, Refined structure of alpha beta-tubulin at 3.5 A resolution, J. Mol. Biol. 313 (5) (2001) 1045–1057.
[11] M.A. Jordan, L. Wilson, Microtubules as a target for anticancer drugs, Nat. Rev. Cancer 4 (4) (2004) 253–265.
[12] R. Bharadwaj, H. Yu, The spindle checkpoint, aneuploidy, and cancer, Oncogene 23 (11) (2004) 2016–2027.

[13] D.A. Brito, Z. Yang, C.L. Rieder, Microtubules do not promote mitotic slippage when the spindle assembly checkpoint cannot be satisfied, J. Cell Biol. 182 (4) (2008) 623–629.
[14] C.D. Scripture, W.D. Figg, A. Sparreboom, Paclitaxel chemotherapy: from empiricism to a mechanism-based formulation strategy, Ther Clin Risk Manag 1 (2) (2005) 107–114.
[15] W.J. Gradishar, Albumin-bound paclitaxel: a next-generation taxane, Expert Opin Pharmacother 7 (8) (2006) 1041–1053.
[16] D.A. Yardley, nab-Paclitaxel mechanisms of action and delivery, J Control Release 170 (3) (2013) 365–372.
[17] N.V. Rajeshkumar, S. Yabuuchi, S.G. Pai, Z. Tong, S. Hou, S. Bateman, D.W. Pierce, C. Heise, D.D. Von Hoff, A. Maitra, et al., Superior therapeutic efficacy of nab-paclitaxel over cremophor-based paclitaxel in locally advanced and metastatic models of human pancreatic cancer, Br. J. Cancer 115 (4) (2016) 442–453.
[18] M.A. Socinski, I. Bondarenko, N.A. Karaseva, A.M. Makhson, I. Vynnychenko, I. Okamoto, J.K. Hon, V. Hirsh, P. Bhar, H. Zhang, et al., Weekly nab-paclitaxel in combination with carboplatin versus solvent-based paclitaxel plus carboplatin as first-line therapy in patients with advanced non-small-cell lung cancer: final results of a phase III trial, J. Clin. Oncol. 30 (17) (2012) 2055–2062.
[19] Q. Song, H. Wang, D. Jiang, C. Xu, J. Cui, Q. Zhang, H. Wang, J. Huang, J. Su, G. S. Wu, et al., Pharmacological inhibition of PP2A overcomes nab-paclitaxel resistance by downregulating MCL1 in esophageal squamous cell carcinoma (ESCC), Cancers 13 (19) (2021).
[20] E. Parasido, G.S. Avetian, A. Naeem, G. Graham, M. Pishvaian, E. Glasgow, S. Mudambi, Y. Lee, C. Ihemelandu, M. Choudhry, et al., The sustained induction of c-MYC drives nab-paclitaxel resistance in primary pancreatic ductal carcinoma cells, Mol. Cancer Res. 17 (9) (2019) 1815–1827.
[21] S. Vallo, R. Köpp, M. Michaelis, F. Rothweiler, G. Bartsch, M.P. Brandt, K.M. Gust, F. Wezel, R.A. Blaheta, A. Haferkamp, et al., Resistance to nanoparticle albumin-bound paclitaxel is mediated by ABCB1 in urothelial cancer cells, Oncol. Lett. 13 (6) (2017) 4085–4092.
[22] F. Skoulidis, L.A. Byers, L. Diao, V.A. Papadimitrakopoulou, P. Tong, J. Izzo, C. Behrens, H. Kadara, E.R. Parra, J.R. Canales, et al., Co-occurring genomic alterations define major subsets of KRAS-mutant lung adenocarcinoma with distinct biology, immune profiles, and therapeutic vulnerabilities, Cancer Discov. 5 (8) (2015) 860–877.
[23] D.E. Jenne, H. Reimann, J. Nezu, W. Friedel, S. Loff, R. Jeschke, O. Müller, W. Back, M. Zimmer, Peutz-Jeghers syndrome is caused by mutations in a novel serine threonine kinase, Nat. Genet. 18 (1) (1998) 38–43.
[24] D.B. Shackelford, R.J. Shaw, The LKB1-AMPK pathway: metabolism and growth control in tumour suppression, Nat. Rev. Cancer 9 (8) (2009) 563–575.
[25] H. Lee, F. Zandkarimi, Y. Zhang, J.K. Meena, J. Kim, L. Zhuang, S. Tyagi, L. Ma, T. F. Westbrook, G.R. Steinberg, et al., Energy-stress-mediated AMPK activation inhibits ferroptosis, Nat. Cell Biol. 22 (2) (2020) 225–234.
[26] S.M. Kim, T.T. Nguyen, A. Ravi, P. Kubiniok, B.T. Finicle, V. Jayashankar, L. Malacrida, J. Hou, J. Robertson, D. Gao, et al., PTEN deficiency and AMPK activation promote nutrient scavenging and anabolism in prostate cancer cells, Cancer Discov. 8 (7) (2018) 866–883.
[27] M. Yan, M.C. Gingras, E.A. Dunlop, Y. Nouët, F. Dupuy, Z. Jalali, E. Possik, B. J. Coull, D. Kharitidi, A.B. Dydensborg, et al., The tumor suppressor folliculin regulates AMPK-dependent metabolic transformation, J. Clin. Investig. 124 (6) (2014) 2640–2650.
[28] N. Malik, B.I. Ferreira, P.E. Hollstein, S.D. Curtis, E. Trefts, S. Weiser Novak, J. Yu, R. Gilson, K. Hellberg, L. Fang, et al., Induction of lysosomal and mitochondrial biogenesis by AMPK phosphorylation of FNIP1, Science 380 (6642) (2023) eabj5559.
[29] T. Zhang, D. Xu, E. Trefts, M. Lv, H. Inuzuka, G. Song, M. Liu, J. Lu, J. Liu, C. Chu, et al., Metabolic orchestration of cell death by AMPK-mediated phosphorylation of RIPK1, Science 380 (6652) (2023) 1372–1380.
[30] J. Chen, L. Zou, G. Lu, O. Grinchuk, L. Fang, D.S.T. Ong, R. Taneja, C.N. Ong, H. M. Shen, PFKP alleviates glucose starvation-induced metabolic stress in lung cancer cells via AMPK-ACC2 dependent fatty acid oxidation, Cell Discov 8 (1) (2022) 52.
[31] A.B. Hwang, E.A. Ryu, M. Artan, H.W. Chang, M.H. Kabir, H.J. Nam, D. Lee, J. S. Yang, S. Kim, W.B. Mair, et al., Feedback regulation via AMPK and HIF-1 mediates ROS-dependent longevity in Caenorhabditis elegans, Proc. Natl. Acad. Sci. U. S. A. 111 (42) (2014) E4458–E4467.
[32] E. Zulato, F. Ciccarese, G. Nardo, M. Pinazza, V. Agnusdei, M. Silic-Benussi, V. Ciminale, S. Indraccolo, Involvement of NADPH oxidase 1 in liver kinase B1-mediated effects on tumor angiogenesis and growth, Front. Oncol. 8 (2018) 195.
[33] R. Li, T.S.C. Ng, S.J. Wang, M. Prytyskach, C.B. Rodell, H. Mikula, R.H. Kohler, M. A. Garlin, D.A. Lauffenburger, S. Parangi, et al., Therapeutically reprogrammed nutrient signalling enhances nanoparticulate albumin bound drug uptake and efficacy in KRAS-mutant cancer, Nat. Nanotechnol. 16 (7) (2021) 830–839.
[34] Y. Diao, X. Ma, W. Min, S. Lin, H. Kang, Z. Dai, X. Wang, Y. Zhao, Dasatinib promotes paclitaxel-induced necroptosis in lung adenocarcinoma with phosphorylated caspase-8 by c-Src, Cancer Lett. 379 (1) (2016) 12–23.
[35] M. Tang, S. Zhao, J.X. Liu, X. Liu, Y.X. Guo, G.Y. Wang, X.L. Wang, Paclitaxel induces cognitive impairment via necroptosis, decreased synaptic plasticity and M1 polarisation of microglia, Pharm. Biol. 60 (1) (2022) 1556–1565.
[36] C.C. Zhang, C.G. Li, Y.F. Wang, L.H. Xu, X.H. He, Q.Z. Zeng, C.Y. Zeng, F.Y. Mai, B. Hu, D.Y. Ouyang, Chemotherapeutic paclitaxel and cisplatin differentially induce pyroptosis in A549 lung cancer cells via caspase-3/GSDME activation, Apoptosis 24 (3–4) (2019) 312–325.
[37] S. Zhao, Y. Tang, R. Wang, M. Najafi, Mechanisms of cancer cell death induction by paclitaxel: an updated review, Apoptosis 27 (9–10) (2022) 647–667.
[38] B.A. Weaver, How Taxol/paclitaxel kills cancer cells, Mol. Biol. Cell 25 (18) (2014) 2677–2681.
[39] M. Saxena, S.A. Balaji, N. Deshpande, S. Ranganathan, D.M. Pillai, S.K. Hindupur, A. Rangarajan, AMP-activated protein kinase promotes epithelial-mesenchymal transition in cancer cells through Twist1 upregulation, J. Cell Sci. 131 (14) (2018).
[40] N. Li, D. Huang, N. Lu, L. Luo, Role of the LKB1/AMPK pathway in tumor invasion and metastasis of cancer cells, Oncol. Rep. 34 (6) (2015) 2821–2826 (Review).
[41] S.A. Hawley, F.M. Russell, F.A. Ross, D.G. Hardie, BAY-3827 and SBI-0206965: potent AMPK inhibitors that paradoxically increase Thr172 phosphorylation, Int. J. Mol. Sci. 25 (1) (2023).
[42] C. Lemos, V.K. Schulze, S.J. Baumgart, E. Nevedomskaya, T. Heinrich, J. Lefranc, B. Bader, C.D. Christ, H. Briem, L.P. Kuhnke, et al., The potent AMPK inhibitor BAY-3827 shows strong efficacy in androgen-dependent prostate cancer models, Cell. Oncol. 44 (3) (2021) 581–594.
[43] J. Kim, G. Yang, Y. Kim, J. Kim, J. Ha, AMPK activators: mechanisms of action and physiological activities, Exp. Mol. Med. 48 (4) (2016) e224.
[44] G. Ceolotto, A. Gallo, I. Papparella, L. Franco, E. Murphy, E. Iori, E. Pagnin, G. P. Fadini, M. Albiero, A. Semplicini, et al., Rosiglitazone reduces glucose-induced oxidative stress mediated by NAD(P)H oxidase via AMPK-dependent mechanism, Arterioscler. Thromb. Vasc. Biol. 27 (12) (2007) 2627–2633.
[45] G. Xia, T. Zhu, X. Li, Y. Jin, J. Zhou, J. Xiao, ROS-mediated autophagy through the AMPK signaling pathway protects INS-1 cells from human islet amyloid polypeptide-induced cytotoxicity, Mol. Med. Rep. 18 (3) (2018) 2744–2752.
[46] Y. Ren, H.M. Shen, Critical role of AMPK in redox regulation under glucose starvation, Redox Biol. 25 (2019) 101154.
[47] X. Ren, B. Zhao, H. Chang, M. Xiao, Y. Wu, Y. Liu, Paclitaxel suppresses proliferation and induces apoptosis through regulation of ROS and the AKT/MAPK signaling pathway in canine mammary gland tumor cells, Mol. Med. Rep. 17 (6) (2018) 8289–8299.
[48] J. Alexandre, Y. Hu, W. Lu, H. Pelicano, P. Huang, Novel action of paclitaxel against cancer cells: bystander effect mediated by reactive oxygen species, Cancer Res. 67 (8) (2007) 3512–3517.
[49] A. Zhitkovich, N-acetylcysteine: antioxidant, aldehyde scavenger, and more, Chem. Res. Toxicol. 32 (7) (2019) 1318–1319.
[50] J. Lu, A. Holmgren, The thioredoxin antioxidant system, Free Radic. Biol. Med. 66 (2014) 75–87.
[51] P. Koppula, L. Zhuang, B. Gan, Cystine transporter SLC7A11/xCT in cancer: ferroptosis, nutrient dependency, and cancer therapy, Protein Cell 12 (8) (2021) 599–620.
[52] U. Anand, A. Dey, A.K.S. Chandel, R. Sanyal, A. Mishra, D.K. Pandey, V. De Falco, A. Upadhyay, R. Kandimalla, A. Chaudhary, et al., Cancer chemotherapy and beyond: current status, drug candidates, associated risks and progress in targeted therapeutics, Genes Dis 10 (4) (2023) 1367–1401.
[53] R.F. Ozols, B.N. Bundy, B.E. Greer, J.M. Fowler, D. Clarke-Pearson, R.A. Burger, R. S. Mannel, K. DeGeest, E.M. Hartenbach, R. Baergen, Phase III trial of carboplatin and paclitaxel compared with cisplatin and paclitaxel in patients with optimally resected stage III ovarian cancer: a Gynecologic Oncology Group study, J. Clin. Oncol. 21 (17) (2003) 3194–3200.
[54] G.V. Kondagunta, J. Bacik, A. Donadio, D. Bajorin, S. Marion, J. Sheinfeld, G. J. Bosl, R.J. Motzer, Combination of paclitaxel, ifosfamide, and cisplatin is an effective second-line therapy for patients with relapsed testicular germ cell tumors, J. Clin. Oncol. 23 (27) (2005) 6549–6555.
[55] B.D. Stein, J.R. Ferrarone, E.E. Gardner, J.W. Chang, D. Wu, P.E. Hollstein, R. J. Liang, M. Yuan, Q. Chen, J.S. Coukos, et al., LKB1-Dependent regulation of TPI1 creates a divergent metabolic liability between human and mouse lung adenocarcinoma, Cancer Discov. 13 (4) (2023) 1002–1025.
[56] J.M. Lizcano, O. Goransson, R. Toth, M. Deak, N.A. Morrice, J. Boudeau, S. A. Hawley, L. Udd, T.P. Makela, D.G. Hardie, et al., LKB1 is a master kinase that activates 13 kinases of the AMPK subfamily, including MARK/PAR-1, EMBO J. 23 (4) (2004) 833–843.
[57] E.I. Tang, D.D. Mruk, C.Y. Cheng, MAP/microtubule affinity-regulating kinases, microtubule dynamics, and spermatogenesis, J. Endocrinol. 217 (2) (2013) R13–R23.
[58] Y. Kojima, H. Miyoshi, H.C. Clevers, M. Oshima, M. Aoki, M.M. Taketo, Suppression of tubulin polymerization by the LKB1-microtubule-associated protein/microtubule affinity-regulating kinase signaling, J. Biol. Chem. 282 (32) (2007) 23532–23540.
[59] I. Mian, W.S. Pierre-Louis, N. Dole, R.M. Gilberti, K. Dodge-Kafka, J.S. Tirnauer, LKB1 destabilizes microtubules in myoblasts and contributes to myoblast differentiation, PLoS One 7 (2) (2012) e31583.
[60] E.C. Hinchy, A.V. Gruszczyk, R. Willows, N. Navaratnam, A.R. Hall, G. Bates, T. P. Bright, T. Krieg, D. Carling, M.P. Murphy, Mitochondria-derived ROS activate AMP-activated protein kinase (AMPK) indirectly, J. Biol. Chem. 293 (44) (2018) 17208–17217.
[61] F.R. Auciello, F.A. Ross, N. Ikematsu, D.G. Hardie, Oxidative stress activates AMPK in cultured cells primarily by increasing cellular AMP and/or ADP, FEBS Lett. 588 (18) (2014) 3361–3366.
[62] J.W. Zmijewski, S. Banerjee, H. Bae, A. Friggeri, E.R. Lazarowski, E. Abraham, Exposure to hydrogen peroxide induces oxidation and activation of AMP-activated protein kinase, J. Biol. Chem. 285 (43) (2010) 33154–33164.
[63] Y. Ren, J. Chen, P. Chen, Q. Hao, L.K. Cheong, M. Tang, L.L. Hong, X.Y. Hu, T. Y. Celestial, B.H. Bay, et al., Oxidative stress-mediated AMPK inactivation determines the high susceptibility of LKB1-mutant NSCLC cells to glucose starvation, Free Radic. Biol. Med. 166 (2021) 128–139.
[64] M. Wu, A. Zhao, X. Yan, H. Gao, C. Zhang, X. Liu, Q. Luo, F. Xie, S. Liu, D. Shi, Hepatic AMPK signaling dynamic activation in response to REDOX balance are

sentinel biomarkers of exercise and antioxidant intervention to improve blood glucose control, Elife 11 (2022).
[65] R.C. Rabinovitch, B. Samborska, B. Faubert, E.H. Ma, S.P. Gravel, S. Andrzejewski, T.C. Raissi, A. Pause, J. St-Pierre, R.G. Jones, AMPK maintains cellular metabolic homeostasis through regulation of mitochondrial reactive oxygen species, Cell Rep. 21 (1) (2017) 1–9.
[66] E. Zulato, F. Ciccarese, V. Agnusdei, M. Pinazza, G. Nardo, E. Iorio, M. Curtarello, M. Silic-Benussi, E. Rossi, C. Venturoli, et al., LKB1 loss is associated with glutathione deficiency under oxidative stress and sensitivity of cancer cells to cytotoxic drugs and γ-irradiation, Biochem. Pharmacol. 156 (2018) 479–490.
[67] X. Song, S. Zhu, P. Chen, W. Hou, Q. Wen, J. Liu, Y. Xie, J. Liu, D.J. Klionsky, G. Kroemer, et al., AMPK-mediated BECN1 phosphorylation promotes ferroptosis by directly blocking system X(c)(-) activity, Curr. Biol. 28 (15) (2018) 2388–2399. e2385.
[68] X. Wang, X. Chen, W. Zhou, H. Men, T. Bao, Y. Sun, Q. Wang, Y. Tan, B.B. Keller, Q. Tong, et al., Ferroptosis is essential for diabetic cardiomyopathy and is prevented by sulforaphane via AMPK/NRF2 pathways, Acta Pharm. Sin. B 12 (2) (2022) 708–722.
[69] Q. Lu, L. Yang, J.J. Xiao, Q. Liu, L. Ni, J.W. Hu, H. Yu, X. Wu, B.F. Zhang, Empagliflozin attenuates the renal tubular ferroptosis in diabetic kidney disease through AMPK/NRF2 pathway, Free Radic. Biol. Med. 195 (2023) 89–102.
[70] Z. Wang, Y. Wang, N. Shen, Y. Liu, X. Xu, R. Zhu, H. Jiang, X. Wu, Y. Wei, J. Tang, AMPKα1-mediated ZDHHC8 phosphorylation promotes the palmitoylation of SLC7A11 to facilitate ferroptosis resistance in glioblastoma, Cancer Lett. 584 (2024) 216619.
[71] N.B. Ruderman, D. Carling, M. Prentki, J.M. Cacicedo, AMPK, insulin resistance, and the metabolic syndrome, J. Clin. Investig. 123 (7) (2013) 2764–2772.